RM L55G26a

NACA

# RESEARCH MEMORANDUM

## A WIND-TUNNEL INVESTIGATION OF A 0.4-SCALE MODEL OF AN ASSAULT-TRANSPORT AIRPLANE WITH BOUNDARY-LAYER CONTROL APPLIED

By Marvin P. Fink, Bennie W. Cocke,
and Stanley Lipson

Langley Aeronautical Laboratory
Langley Field, Va.

NATIONAL ADVISORY COMMITTEE
FOR AERONAUTICS

WASHINGTON

May 7, 1956

NATIONAL ADVISORY COMMITTEE FOR AERONAUTICS

RESEARCH MEMORANDUM

# A WIND-TUNNEL INVESTIGATION OF A 0.4-SCALE MODEL OF AN ASSAULT-TRANSPORT AIRPLANE WITH BOUNDARY-LAYER CONTROL APPLIED[1]

By Marvin P. Fink, Bennie W. Cocke, and Stanley Lipson

## SUMMARY

A 0.4-scale powered model of an assault-transport-type airplane equipped with a boundary-layer-control system has been tested in the Langley full-scale tunnel. This program was directed toward evaluating the lift, drag, and lateral and longitudinal stability and control characteristics of the model with boundary-layer control applied, to aid in the design of a flight installation.

With the model boundary-layer-control system operating at design flow rates, maximum lift coefficients (untrimmed) of 3.5 and 4.8 were obtained for the idle and full-power propeller operating conditions. The model was longitudinally stable for all conditions and the elevators appeared to be capable of trimming the model at all conditions for the normal center of gravity (0.27 mean aerodynamic chord).

Aileron effectiveness seemed adequate for all conditions but high adverse yaw was associated with large aileron deflections. The rudder was not adequate for trim on single-engine asymmetric power.

## INTRODUCTION

An investigation has been conducted in the Langley full-scale tunnel to evaluate the effectiveness of a boundary-layer-control system on a 0.4-scale model of an assault-transport airplane. The boundary-layer-control system chosen for this program utilized a single pump to suck air in from the inboard flaps and discharge the same air over the outboard-flap segment and the drooped aileron through a blowing slot.

---

[1]The information presented herein was previously made available to the U. S. military air services.

This investigation included the effects of such variables as flap hinge position, suction slot design, quantity of air handled, nacelle configuration, flap deflection, and propeller operation on the lifting effectiveness of the boundary-layer-control system. Longitudinal and lateral control effectiveness was also evaluated. Included in the control tests were the effects of asymmetric propeller operation and asymmetric boundary-layer-control application. This wind-tunnel investigation, although quite extensive was not given sufficient scope to make a complete flying qualities analysis. The main emphasis was on lift effectiveness with spot evaluation of control effectiveness.

The model tested had a 45-foot wing span, NACA 23017 airfoil section from root to tip, an aspect ratio of 9.7, and a taper ratio of 0.51. Tests were made at a Reynolds number of $1.9 \times 10^6$ and $1.3 \times 10^6$ for the power-off and power-on conditions respectively.

## SYMBOLS

The stability axis system and sign convention used in presenting these data are shown in figure 1.

$C_L$ lift coefficient, $\frac{\text{Lift}}{q_o S}$

$C_D$ drag coefficient, $\frac{\text{Drag}}{q_o S}$

$C_X$ longitudinal-force coefficient, $\frac{\text{Longitudinal force}}{q_o S}$

$C_Y$ lateral-force coefficient, $\frac{\text{Side force}}{q_o S}$

$C_m$ pitching-moment coefficient, $\frac{\text{Pitching moment}}{q_o S \bar{c}}$

$C_n$ yawing-moment coefficient, $\frac{\text{Yawing moment}}{q_o S b}$

$C_l$ rolling-moment coefficient, $\frac{\text{Rolling moment}}{q_o Sb}$

$C_{Q_S}$ suction-flow coefficient, $\frac{Q}{V_o S_s}$

$C_{Q_B}$ blowing-flow coefficient, $\frac{Q}{V_o S_B}$

$S$ wing area, sq ft

$S_s$ wing area affected by suction, sq ft

$S_B$ wing area affected by blowing, sq ft

$c$ local airfoil chord, ft

$\bar{c}$ wing mean aerodynamic chord, ft

$q_o$ free-stream dynamic pressure, lb/sq ft

$\rho$ mass density, slugs/cu ft

$V_o$ free-stream velocity, ft/sec

$T_c'$ thrust coefficient, $\frac{\text{Thrust}}{q_o S}$

$Q$ quantity of air sucked or blown, cu ft/sec

$\psi$ angle of yaw, deg

$\alpha$ angle of attack, deg

$\delta$ control deflection, deg; aileron and flap are positive down, rudder is positive left

$i_t$ incidence of horizontal stabilizer, deg

| | |
|---|---|
| $b/2$ | wing semispan, ft |
| R | free-stream Reynolds number based on the mean aerodynamic chord |
| $dC_m/di_t$ | tail effectiveness parameter |
| $dC_m/d\delta_e$ | elevator effectiveness parameter |
| $dC_l/d\delta_a$ | aileron effectiveness parameter |
| $dC_n/d\delta_r$ | rudder effectiveness parameter |

Subscripts:

| | |
|---|---|
| a | aileron |
| r | rudder |
| f | flaps |
| e | elevator |

## MODEL AND TESTS

### Model

The model tested was a 0.4-scale powered model of an assault-transport-type airplane. The model had a 45-foot wing span, 31-foot length, and 208.67 square feet of wing area. The wing had an NACA 23017 airfoil section and a taper ratio of 0.51, and was attached to the fuselage at an angle of incidence of 7°. The wing was twisted 4° (washout) from root to the tip and had zero sweep at the 0.25c line. The model dimensions and geometric characteristics are shown in figure 2.

The wing was fitted with single slotted 0.25c flaps. Suction was applied to the inboard and center sections. Blowing was applied to the outboard-flap section and aileron. (See fig. 2.) The ailerons extended from 0.60b/2 to 0.975b/2 and were designed on the airplane to droop to 30° when the flaps were deflected to 50°. From this position the ailerons had a deflection range of 20° up to 15° down. The nacelles could be fitted with long or short afterbodies (fig. 2). With the short nacelle installed, a 0.09b/2 portion of the trailing edge spanned by the nacelle would deflect with the flaps and would be affected by suction. With the long nacelle installed, the trailing edge did not

deflect and the suction slot across the nacelle was sealed. Inclosed in each nacelle was a 200-horsepower electric motor to provide power for the test propellers which were two-blade, 76-inch-diameter fixed-pitch propellers with a blade angle of 24° at 0.75 radius station.

Installed in the fuselage (to serve as an air pump for the boundary-layer-control system) was a T31 turbopropeller engine compressor driven through the propeller reduction gearbox by an electric motor. The intake side of the compressor was ducted to the suction slot and the exit side to the blowing slot. Provision was made in the suction system for controlling the quantity of suction air by throttling auxiliary air supply from an external scoop on top of the fuselage. The compressor was modified for the test so that it would pump 209 cu ft/sec at a pressure ratio of 1.2.

## Tests

Tests of the model mounted on the mechanical balance system in the Langley full-scale tunnel (fig. 3), were made primarily in two phases. One was to obtain the effects of several configuration changes including the effects of boundary-layer control on maximum lift, and the other was to determine some of the longitudinal and lateral characteristics of the model for the high-lift configuration.

In the first tests, lift, drag, and pitching-moment data were measured over the angle-of-attack range from -12° to 16° for several flap and aileron configurations without boundary-layer control and for one configuration with boundary-layer control applied. These configurations are designated as follows: A, flap and ailerons neutral; B, flap 50° and ailerons neutral; C, flaps 50°, ailerons 30°; and D, flaps 50°, ailerons 30° with boundary-layer control applied. On configuration D the boundary-layer-control system was operated over a range of flow quantities from 0 to the maximum output of the pump with equal quantities of air being sucked in at the flap juncture and blown out over the outboard flap and aileron, and also for a variation of the relative quantities of the air sucked and blown. These variations were accomplished by setting the desired quantity of blowing air by controlling the compressor rotational speed and regulating the suction air quantity by the bleed valve in the auxiliary air duct. As part of the boundary-layer-control investigation, tests of several hinge-point locations for the blowing flap and aileron, as well as tests of five suction-slot-entrance modifications (fig. 4) for the suction flap were made. Included in the flapped configuration were tests of two nacelle lengths to determine whether or not there was any advantage in lift from using a short nacelle whose aft section could be deflected with the trailing-edge flaps.

Propeller operating conditions from windmilling to a relative high thrust coefficient were investigated for model configurations B, C, and D. Asymmetric power conditions (one propeller windmilling and the other full power) for configuration D, were also tested. For the windmilling propeller and for the low thrust conditions, the tests were made at a Reynolds number of $1.9 \times 10^6$ and for high thrust of $1.3 \times 10^6$ based on a mean aerodynamic chord of 4.64 feet.

In the stability investigation, longitudinal data were obtained for two stabilizer-incidence settings and with the horizontal tail removed for configurations A, B, C, and D. Elevator-, aileron-, and rudder-effectiveness data were obtained, however, for configuration D only. Complete control-effectiveness data were obtained over the angle-of-attack range at zero yaw and data for the aileron and rudder were obtained also at $\psi = 9.85^\circ$. The effects of power on the longitudinal and lateral characteristics of the controls were investigated for a range of propeller operating conditions including windmilling propeller, full power, asymmetric power, and for asymmetric boundary-layer-control operation. The range of control deflection for the respective controls was as follows: elevator from 20° down to 15° up; aileron (from the drooped position, 30° down), 15° down to 20° up; and rudder, 25° right to 25° left.

## PRESENTATION OF DATA

The data from these tests have been corrected for airstream misalinement, and buoyancy effects. Wind-tunnel jet boundary corrections based on actual span loadings and derived according to reference 1 have been applied. In order to present only the aerodynamic drag of the model for power-on conditions, values of thrust coefficient $T_c'$ determined for the tunnel tests have been added to the measured drag for all full-power and idle-power test conditions.

It should be pointed out that the thrust coefficient-lift coefficient relationship used for model tests represents an airplane gross weight of approximately 39,000 pounds for the military power condition. As this gross weight is in the lower weight range of the present airplane (design maximum gross weight 52,600 pounds) the conversion of certain model longitudinal data to thrust conditions representing the higher gross weight may be of interest. Figure 5(a) has therefore been prepared to illustrate the difference in the relationship of $T_c'$ to $C_L$ for the airplane at the two weights and figure 5(b) shows the effects on model characteristics produced by changing the thrust-lift simulation. Figure 5(b), based on model thrust calibration polars, may be used as indicated on the figure to convert the model test data (full-power conditions) to the higher gross-weight thrust simulation.

The data of this investigation are presented as follows:



## RESULTS AND DISCUSSION

### Lift Characteristics

The basic airplane with windmilling propellers and flaps and ailerons neutral (configuration A) reached maximum lift ($C_L = 1.42$, fig. 6(a)) at about 10° angle of attack. Deflection of the flaps to 50° (configuration B, fig. 6(b)) produced a lift-coefficient increase of 0.43, and configuration C with flaps 50° and ailerons drooped 30° showed an increase in the maximum lift coefficient of 0.60 over configuration A, reaching a maximum lift coefficient of 2.02, (fig. 6(c)). The addition of boundary-layer control (configuration D) (fig. 6(d))

operating at the maximum design flow rate ($C_{Q_S} = 0.035$, $C_{Q_B} = 0.023$) increased the maximum lift coefficient for the windmilling propeller condition to about 2.76, thus more than doubling the lift increment produced by flap and aileron deflection at maximum lift. Neither flap deflection nor boundary-layer control produced any appreciable change in lift-curve slope.

Comparison of the data (fig. 6) for the propeller-removed and propeller-windmilling conditions indicates that the windmilling propeller had little effect on lift for angles of attack below stall but did increase the maximum lift coefficient by approximately 0.1 for configurations A, B, and C. For configuration D with boundary-layer control applied, lift was not significantly affected.

Data obtained for configuration D with propeller idling ($T_c'$ approx. 0.25 at $C_{L_{max}}$) show a pronounced increase in the slope of the lift curve resulting in an increase of maximum lift coefficient to approximately 3.5 for an increase of approximately 0.74. This lift increase results primarily from propeller slipstream improving the flow conditions on the wing in the region of the nacelles. Tuft studies for propeller-removed and windmill-propeller conditions showed very rough flow at the wing and nacelle junctures at low angles of attack which induced stall of the suction flap and inboard-wing sections at an angle of attack of approximately $7^\circ$ to $8^\circ$.

Full-power propeller operation, as would be expected, produced sizable lift-coefficient increments for all model configurations (fig. 6) and a maximum lift coefficient of 4.8 was reached for the highest boundary-layer control ($C_{Q_S} = 0.035$, $C_{Q_B} = 0.023$) and highest power conditions ($T_c' = 1.9$) tested. Comparing the lift-coefficient increments due to full-power operation at equal model lift coefficients (equal $T_c'$) for configurations B, C, and D and accounting for differences in angle-of-thrust-vector inclination (differences in model angle of attack) indicates that propeller slipstream had approximately the same effect with or without boundary-layer control operating. For example, at a lift coefficient of 3.0 ($T_c' = 1.1$) the lift increment due to slipstream was approximately 0.9 for configurations B, C, and D. The manner in which boundary-layer control and propeller operation affect span loading is indicated in the plot of section normal force across the left wing semispan (fig. 13). It is interesting to note that increments in $c_n$ due to boundary-layer control over the outboard wing sections (blowing sections) are slightly higher than the increments for the inboard (suction) sections. Also shown is the large increase in loading around the nacelles inboard due to propeller slipstream at full power.

It is possible, however, that the effectiveness of the suction flaps was unduly penalized by the discontinuity in span loading caused by the nacelle afterbody. As indicated by the unsteady action of tufts on the ends of the deflected inboard flaps maximum flow clean-up was not achieved, thereby indicating that the full potential-flow effectiveness of the flap segments was not realized.

Reynolds number.- In order to determine whether or not any significant Reynolds number effects were experienced by the model, a range of Reynolds number from $1.3 \times 10^6$ to $3.1 \times 10^6$ was run for configuration C. Data were also obtained for configuration D at Reynolds number of $1.3 \times 10^6$ and $1.9 \times 10^6$ to show any change in effect due to boundary-layer control. The results of these tests (fig. 7) indicate a small effect on lift coefficient over the angle-of-attack range and an increase in the maximum lift coefficient of about 0.1 from a Reynolds number of $1.3 \times 10^6$ to a Reynolds number of $1.9 \times 10^6$. There seemed to be no appreciable difference between the effects of Reynolds number with or without boundary-layer control. The higher Reynolds number had slightly lower drag coefficients over the angle-of-attack range.

Effect of nacelle length.- In view of the fact that the nacelles are used for fuel storage, it was of interest to determine whether or not any aerodynamic advantage gained by a short nacelle (for the landing configuration) would warrant the sacrifice of fuel capacity. The results of these tests (fig. 8) show that for configuration A the long nacelle gave slightly higher lift coefficients and slightly lower drag coefficients over the angle-of-attack range than the short nacelle. On the flapped configurations, however, (configurations B and C) where maximum lift is the prime consideration the short nacelle shows only slightly higher lift coefficient and about the same drag as the long nacelle. With the application of boundary-layer control (configuration D), the short nacelle (fig. 8) showed an incremental lift increase of $C_{l_{max}}$ of 0.2 over the long nacelle when the two are compared at $C_{Q_S} = 0.025$. It must be noted here, however, that even though the shorter nacelle showed a higher lift increment for this condition it also required more power to operate the boundary-layer-control system because the short nacelle had a longer span with suction applied and required more total flow quantity to obtain equal $C_{Q_S}$ based on affected wing area. When the nacelles are compared on the basis of equal absolute flow quantity represented by $C_{Q_S} = 0.025$ and $C_{Q_S} = 0.035$, figure 8, for the short and long nacelles, respectively, it is seen that maximum lift characteristics are almost identical.

Effect of blowing-flap hinge position.- In an effort to determine whether or not the "normal" hinge position for the blowing flap and aileron

was the best of the three positions provided, tests were conducted for two additional hinge positions designated as low and aft, respectively. These data (fig. 9) indicate that the normal hinge position is more effective than the others tested. Also, for all hinge positions, increasing flap or aileron deflections beyond design values ($\delta_a = 30^\circ$, $\delta_f = 50^\circ$) produced only small lift improvement at maximum lift.

Effect of suction - slot modification.- The maximum lift coefficient obtainable was not greatly affected by any of the suction-slot modifications shown in figure 3. These data are summarized in figure 10.

Effect of flow-coefficient variation.- Results of tests made to determine the effect of total quantity flow variation for the boundary-layer-control system from zero flow to full capacity of the model's blowing equipment are shown in figure 11(a) and summarized in figure 11(b). These data representing equal quantity flow through suction and blowing slots show that lift coefficient increased linearly with flow coefficient through most of the range studied but showed definite signs of slope reduction for flow-coefficient values just above airplane design values ($C_{Q_S} = 0.025$, $C_{Q_B} = 0.023$ for short nacelle configuration). The variation of $\Delta C_L$ with flow quantity (fig. 11(b)) is approximately the same for angles of attack up to maximum lift with $\Delta C_L$ of approximately 1.0 shown for the design boundary-layer-control condition. At maximum lift, $\Delta C_L$ values were somewhat lower for all flow conditions.

Results of tests made with suction- and blowing-flow rates varied with respect to one another are shown in figure 12. As would be expected from theory and previous results for suction and blowing boundary-layer-control applications to trailing-edge flaps, lift increments due to increased suction flow rates diminished for flow rates above approximately $C_{Q_S} = 0.025$ while increasing blowing-flow coefficients continued to produce lift increases throughout the range studied.

## Longitudinal Characteristics

Longitudinal data for the various model configurations (A, B, C, and D) with propellers windmilling, and for configuration D with idle-power and full-power thrust conditions (fig. 14) indicate that the model is statically stable for all flap and power configurations tested. For configurations A, B, and C without boundary-layer control the flap or aileron deflection had little effect on stability with average values of $dC_m/dC_L$ being approximately -0.25 for the low angle-of-attack range and increasing to approximately -0.34 for high angles of attack. For configuration D (boundary-layer control applied) with propeller windmilling, stability was increased with values of $dC_m/dC_L$ increased to

approximately -0.32 and -0.44 for the low and high angle-of-attack ranges, respectively. The effect of propeller operation for configuration D was to reduce static stability with values of $dC_m/dC_L$ for the full power condition being approximately half the values for the windmill power condition.

Stabilizer-effectiveness data also presented in figure 14 indicate only moderate changes in effectiveness $\frac{dC_m}{di_t}$ with either model configuration or lift coefficient for the propeller-windmilling condition. Effectiveness data summarized in figure 16(b) for configuration D show that idling propeller causes a reduction of $\frac{dC_m}{di_t}$ from -0.051 to -0.033 at the low angle-of-attack range while in the moderate to high angle-of-attack range propeller operation has very little effect on stabilizer effectiveness with an average value of about -0.052 obtained. The change in stabilizer incidence from 3° to -3° with the elevator neutral was sufficient to produce trim to $C_{L_{max}}$ for configurations A, B, and C with propeller windmilling but was not sufficient to trim to $C_{L_{max}}$ for any power condition with boundary-layer control applied (configuration D).

Elevator effectiveness.- The elevator-effectiveness data for configuration D with boundary-layer control applied (figs. 15 and 16) indicate that for the normal center-of-gravity position (27 percent $\bar{c}$) the elevator is capable of trim at $C_{L_{max}}$ for either the windmill or full-power conditions with a lift-coefficient decrement for trim of about 0.2. Elevator-effectiveness data summarized in figure 16 show only slight change in effectiveness due to propeller slipstream. Calculations based on test results indicate that the elevator alone for fixed stabilizer ($i_t = 3°$) will not provide trim to $C_{L_{max}}$ for center-of-gravity positions forward of 24 percent $\bar{c}$ neglecting effects of landing gear not represented in these tests.

## Lateral Characteristics

Aileron effectiveness.- The aileron effectiveness obtained from figure 17 and summarized in figure 18 (based on total aileron movement (up + down)) was approximately constant through the angle-of-attack range up to stall and was only slightly affected by propeller operation. Even for asymmetric power or asymmetric boundary-layer-control operation, aileron effectiveness was relatively unchanged and the aileron should be able to trim the airplane to angles of attack within a few degrees of maximum lift for the asymmetric power condition. It should be noted, however, that the adverse yaw associated with large aileron deflections (see fig. 17) is rather significant.

Rudder effectiveness.- The rudder maintains reasonable effectiveness through the angle-of-attack range to $C_{L_{max}}$ and is not greatly affected by propeller operation. For the zero yaw condition (figs. 19 and 21(a)) values of $\frac{dC_n}{d\delta_r}$ varied between -0.0012 and -0.0008 for the angle-of-attack range from -8° to +8°. For the yawed condtion (figs. 20 and 21(b)) $\frac{dC_n}{d\delta_r}$ generally ranged between -0.001 and -0.0015 for the three propeller-operating conditions.

The data for zero yaw (fig. 19) indicate that for the asymmetric power condition (one engine windmilling, one engine full power) the rudder is not capable of providing trim except at the lowest angle of attack tested ($\alpha$ = -10°, $C_L$ = 1.02). Even with the model at $\psi$ = 9.85° trim was possible only at the lowest angles of attack tested. It should be noted that these conditions are more severe than will be experienced by the airplane due to the higher single-engine thrust represented by the tunnel tests; however, approximate calculations indicate that trim would not have been achieved for angles of attack higher than approximately -3° ($C_L$ = 2.1) with airplane single-engine rated-thrust applied.

It should also be noted that the adverse yaw associated with large aileron deflections for the airplane with boundary-layer control operating (fig. 17) is of sufficient magnitude at high angles of attack to approach or exceed in some instances the trim capabilities of the rudder at full deflection, and this does not include additional rudder requirement to trim the yaw due to roll.

## CONCLUSIONS

The results of an investigation to determine the maximum lift and static stability characteristics of a 0.4-scale (powered) model of an assault-transport airplane incorporating boundary-layer control are presented as follows:

1. Operating the boundary-layer-control system on the model at design flow rates increased the maximum lift coefficient for the windmill-power condition (flaps deflected 50°, ailerons deflected 30°) from 2.0 to 2.76.

2. Propeller operation improved the flow around the nacelles and produced untrimmed maximum lift values of 3.5 and 4.8 (with boundary-layer control) for the idle-power ($T_c'$ = 0.25) and full-power ($T_c'$ = 1.9) conditions, respectively.

3. For the basic clean model configuration (all controls and flaps neutral) the wing with the long nacelle had better lift and drag characteristics than the wing with the short nacelle. For the landing condition, with flaps deflected and boundary-layer control operating at design flow rates, each nacelle configuration produced about the same wing aerodynamic characteristics.

4. For the condition of equal quantities of flow through the suction and blowing slots the lift coefficient increased linearly with flow coefficient through the flow range tested up to airplane design values.

5. The model with or without boundary-layer control was statically stable longitudinally for all model configurations and propeller-operating conditions. Boundary-layer-control application caused a moderate increase in the basic airplane stability.

6. The effect of full-power operation on the static stability of the model was to reduce the values of $dC_m/dC_L$ obtained for the windmill-power conditions by about half, with values of about -0.17 and -0.26 for the low and high angles of attack, respectively.

7. Elevator effectiveness was not appreciably affected by propeller operation and was nearly constant over the angle-of-attack range, with slight reductions in the high angle-of-attack range. The elevator was capable of trimming the model over the $C_L$ range with the center of gravity located at 0.27 mean aerodynamic chord.

8. Aileron effectiveness was nearly constant over the angle-of-attack range and was only slightly affected by propeller operation. The ailerons appeared to be capable of trimming the airplane for asymmetric power to within a few degrees of $C_{L_{max}}$. Large adverse yawing moments were associated with large aileron deflections.

9. Rudder effectiveness was not appreciably affected by angle-of-attack change or propeller operation with $dC_n/d\delta_r$ varying from -0.0008 to -0.0014. The existing rudder did not appear to be sufficient to provide trim for single-engine operation and may be marginal for trimming the high adverse yaw due to large aileron deflections.

Langley Aeronautical Laboratory,
National Advisory Committee for Aeronautics,
Langley Field, Va., July 25, 1955.

## REFERENCE

1. Katzoff, S., and Hannah, Margery E.: Calculation of Tunnel-Induced Upwash Velocities for Swept and Yawed Wings. NACA TN 1748, 1948.

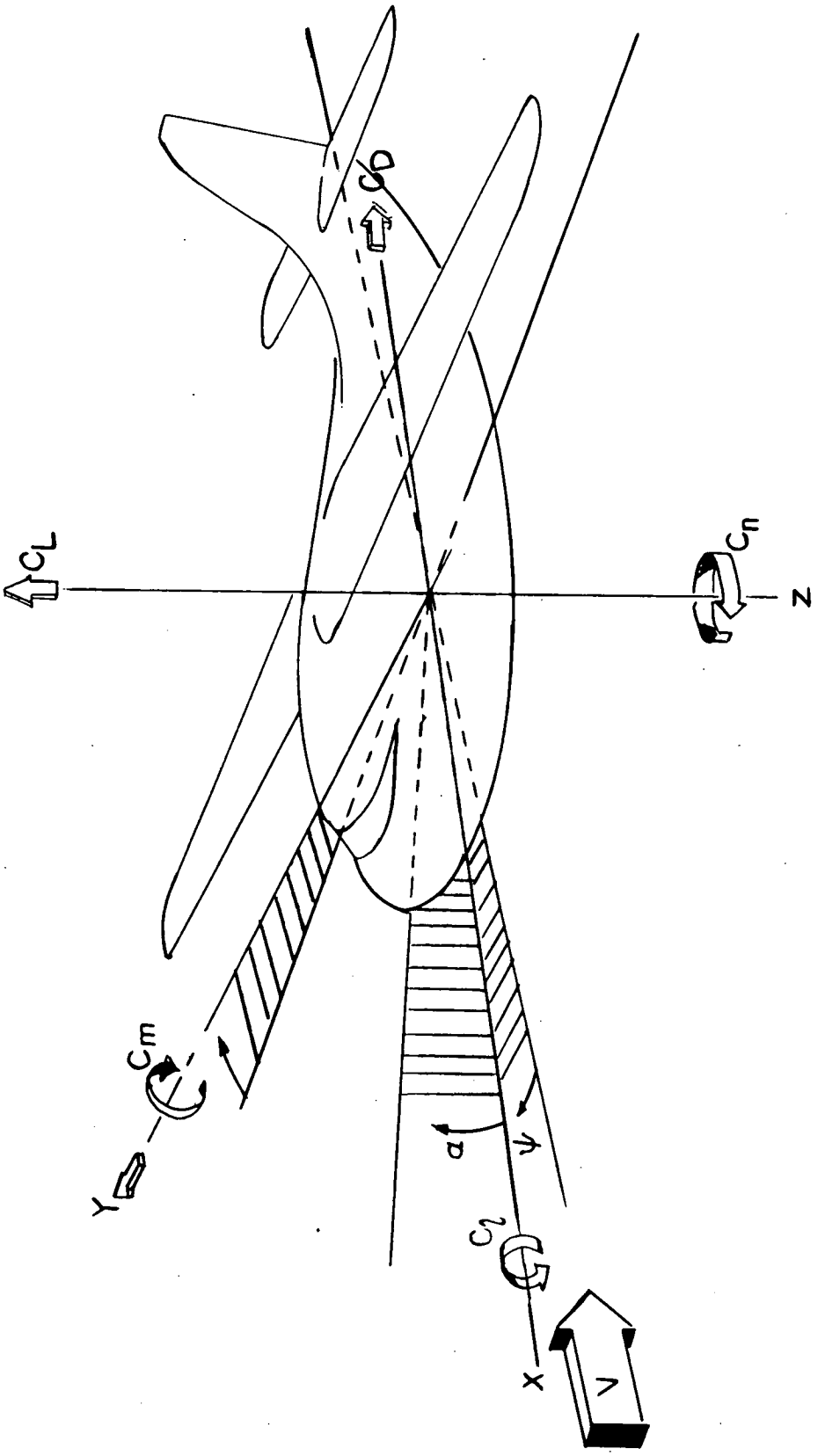


Figure 1.- System of axes used. Arrows indicate positive direction of forces and moments.

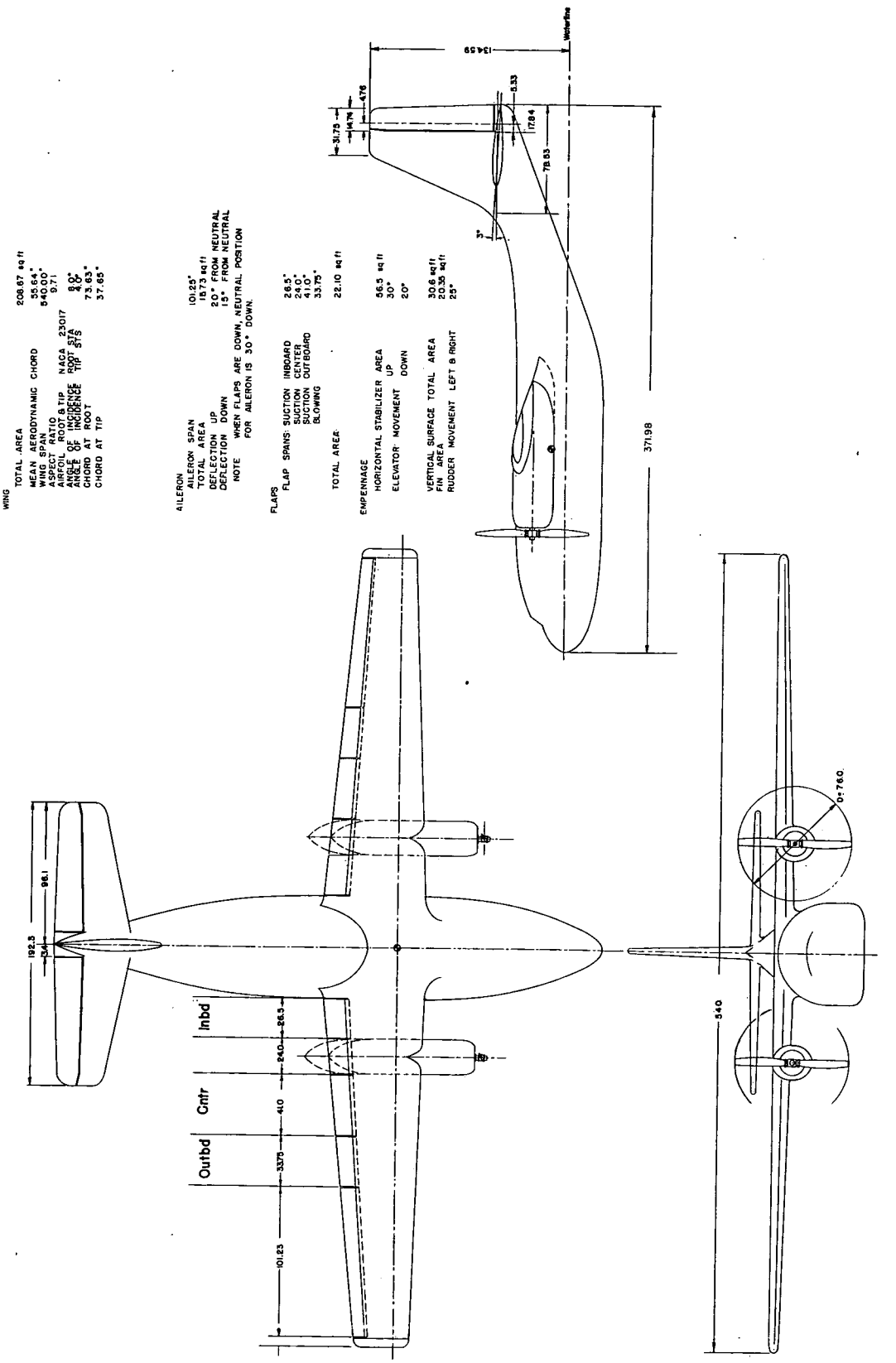


Figure 2.- General layout and principal dimensions of the model. All dimensions are in inches.

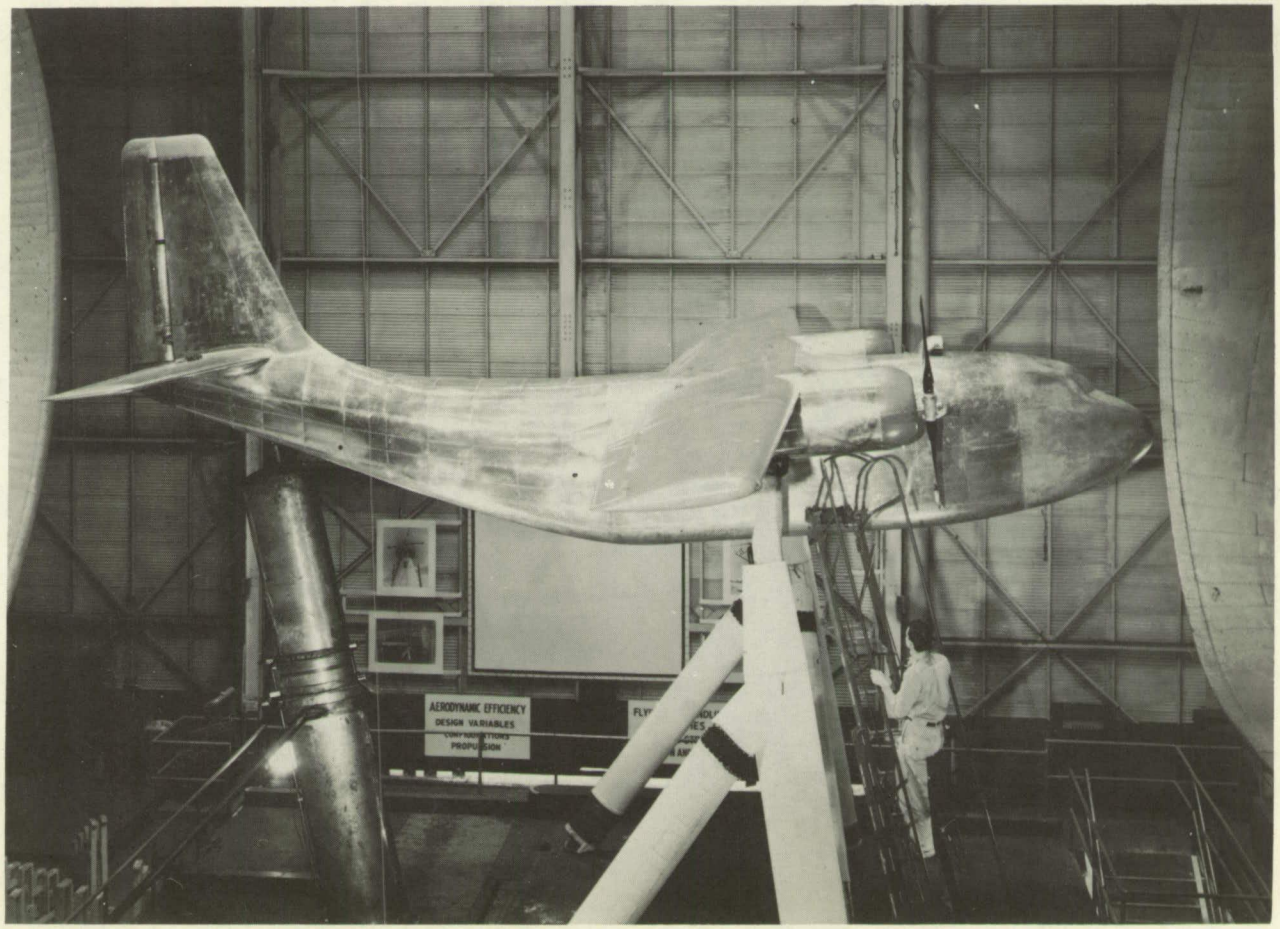


L-79949

(a) General view of model in tunnel.

Figure 3.- General view and closeup photograph of model tested in the Langley full-scale tunnel.

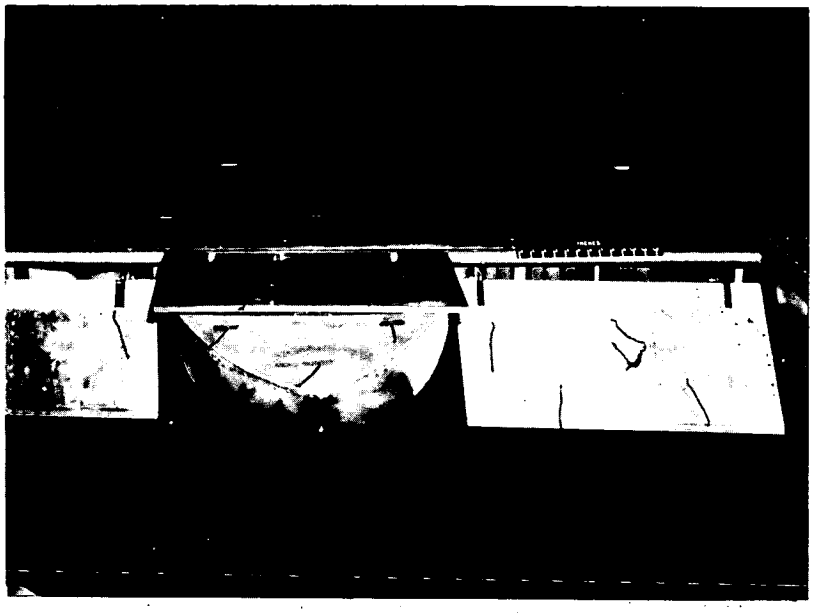

L-80822

Suction flap deflected

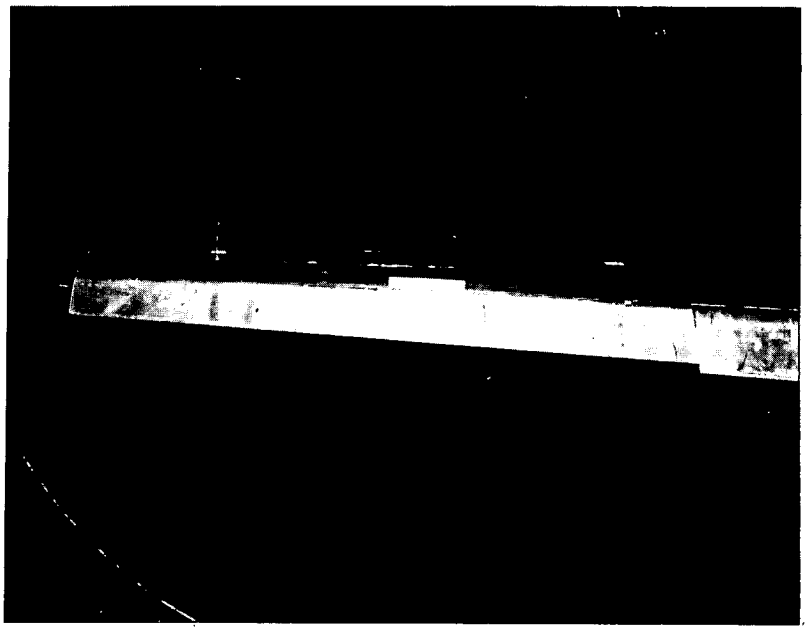

L-80825

Blowing flap and aileron deflected

(b) Close-up photograph of suction flap, blowing flap and aileron.

Figure 3.- Concluded.

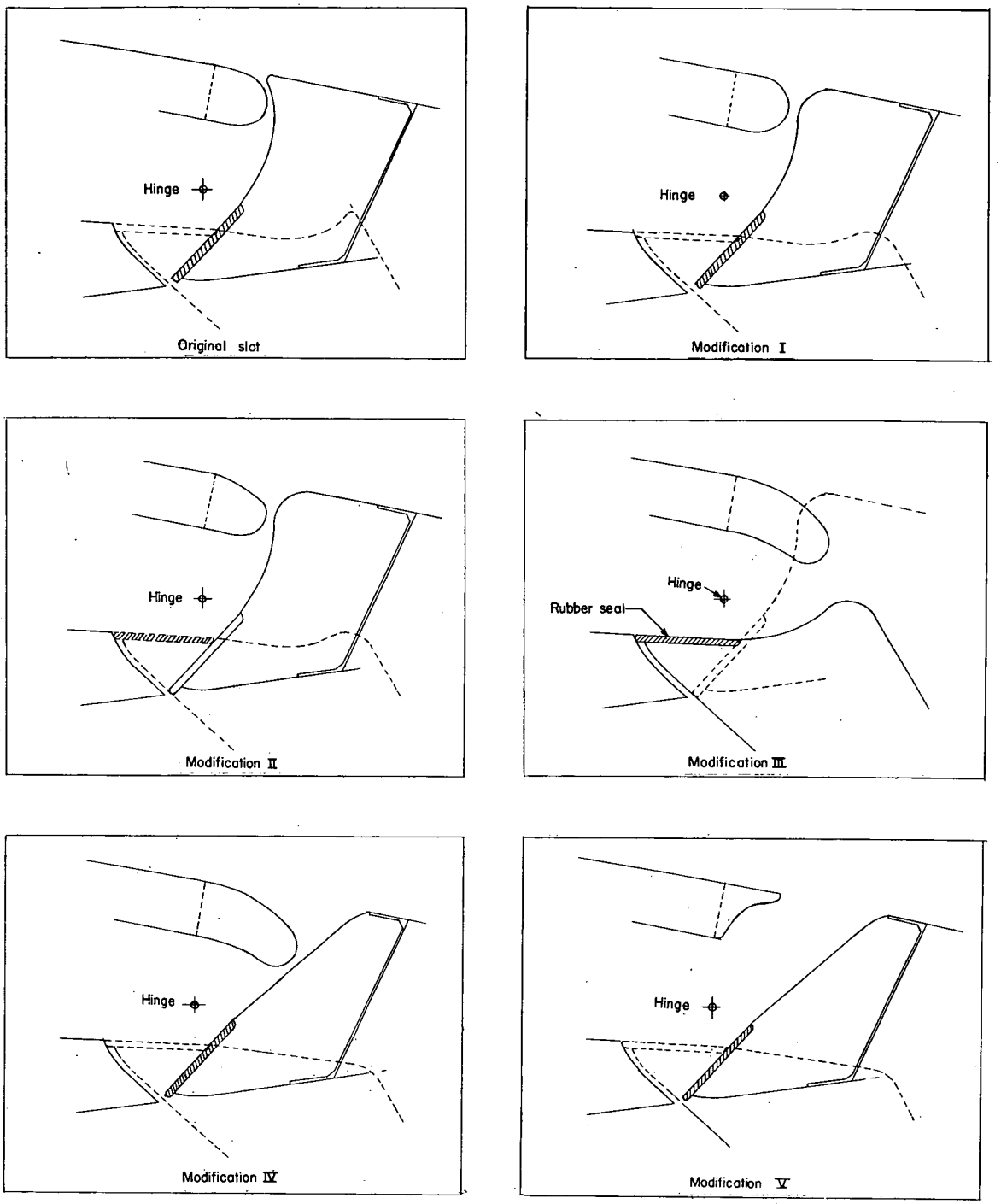


Figure 4.- Suction-slot modifications.

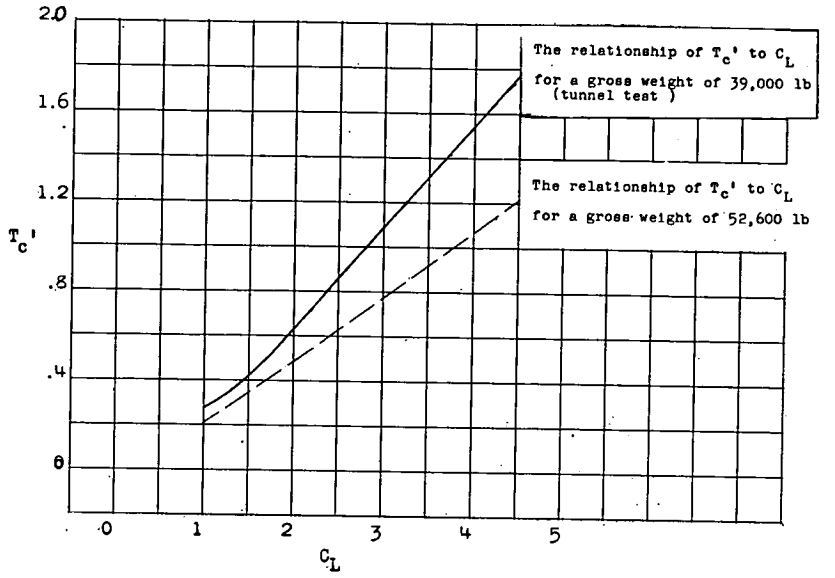


(a) Variation of thrust coefficient with lift coefficient.

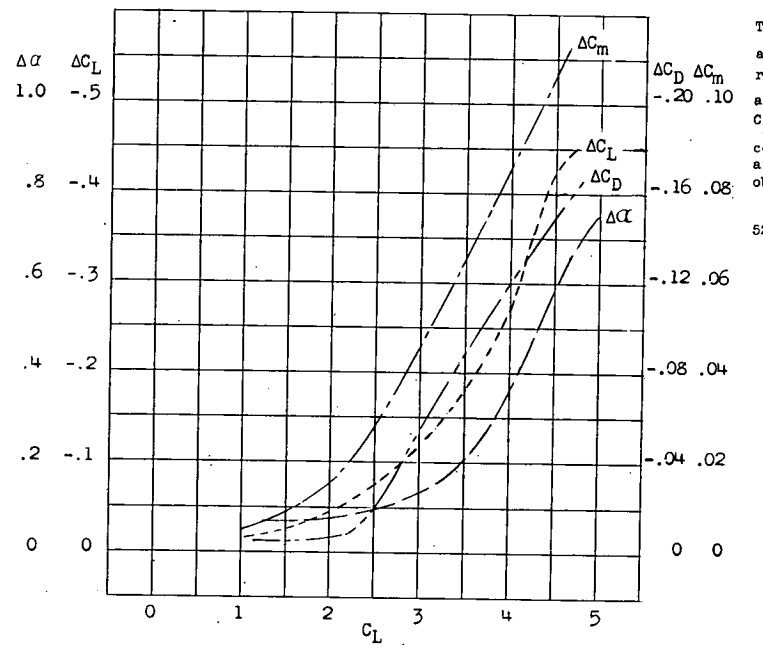


To determine increments of $C_L$, $C_D$, $C_m$, and $\alpha$ for adjusting model data to the relationship of $T_c'$ to $C_L$ representing a 52,600-lb gross weight, take model test $C_L$ values and read increments for each coefficient. Values for the 52,600-lb airplane thrust simulation will then be obtained by the following relationship:

| 52,600 lb | | 39,000 lb |
|---|---|---|
| $C_L$ | = | $C_L + \Delta C_L$ |
| $C_D$ | = | $C_D + \Delta C_D$ |
| $C_m$ | = | $C_m + \Delta C_m$ |
| $\alpha$ | = | $\alpha + \Delta\alpha$ |

(b) Increments for making weight adjustments.

Figure 5.- The relationship of $T_c'$ to $C_L$ for the airplane for two gross weights, and increments for adjusting tunnel test data to the relationship of $T_c'$ to $C_L$ corresponding to the airplane with a gross weight of 52,600 pounds.

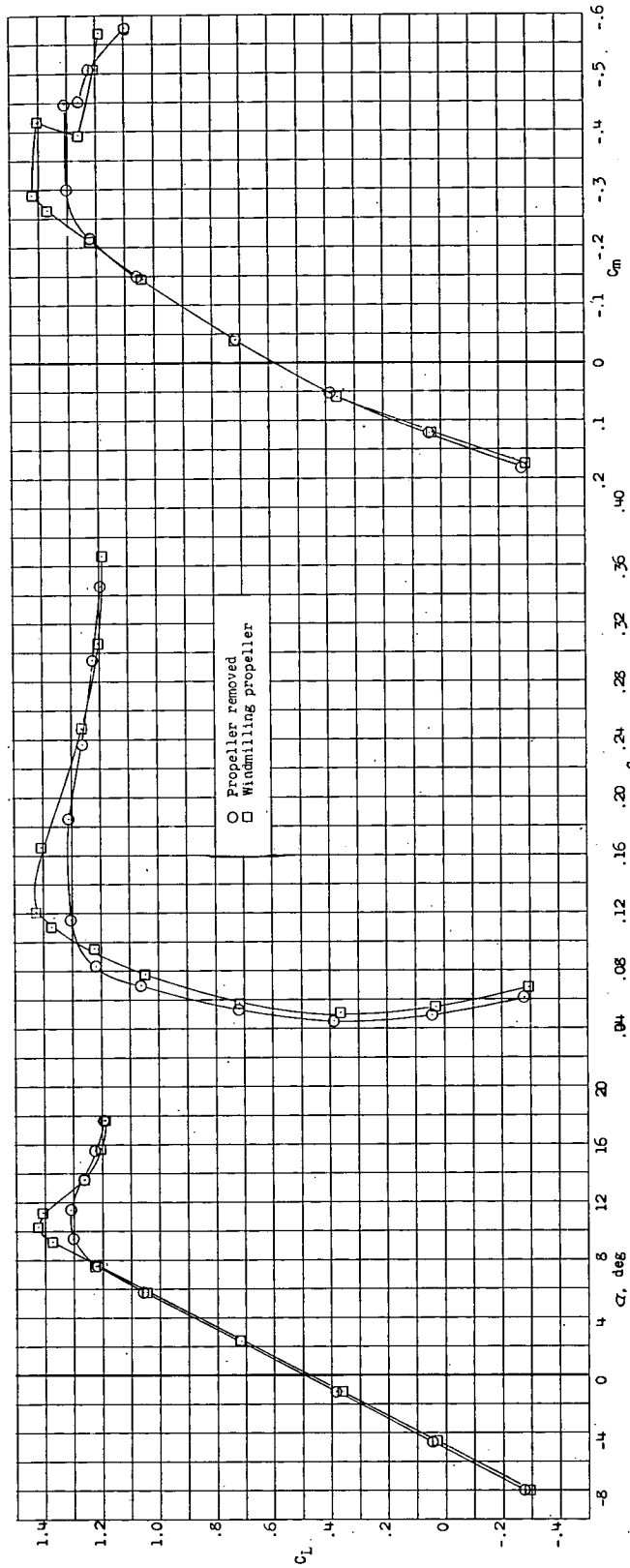


(a) Configuration A. Long nacelle; $C_{Q_S} = 0$; $C_{Q_B} = 0$; $R = 1.9 \times 10^6$.

Figure 6.- Longitudinal characteristics of the four model configurations including the effects of propeller operation.

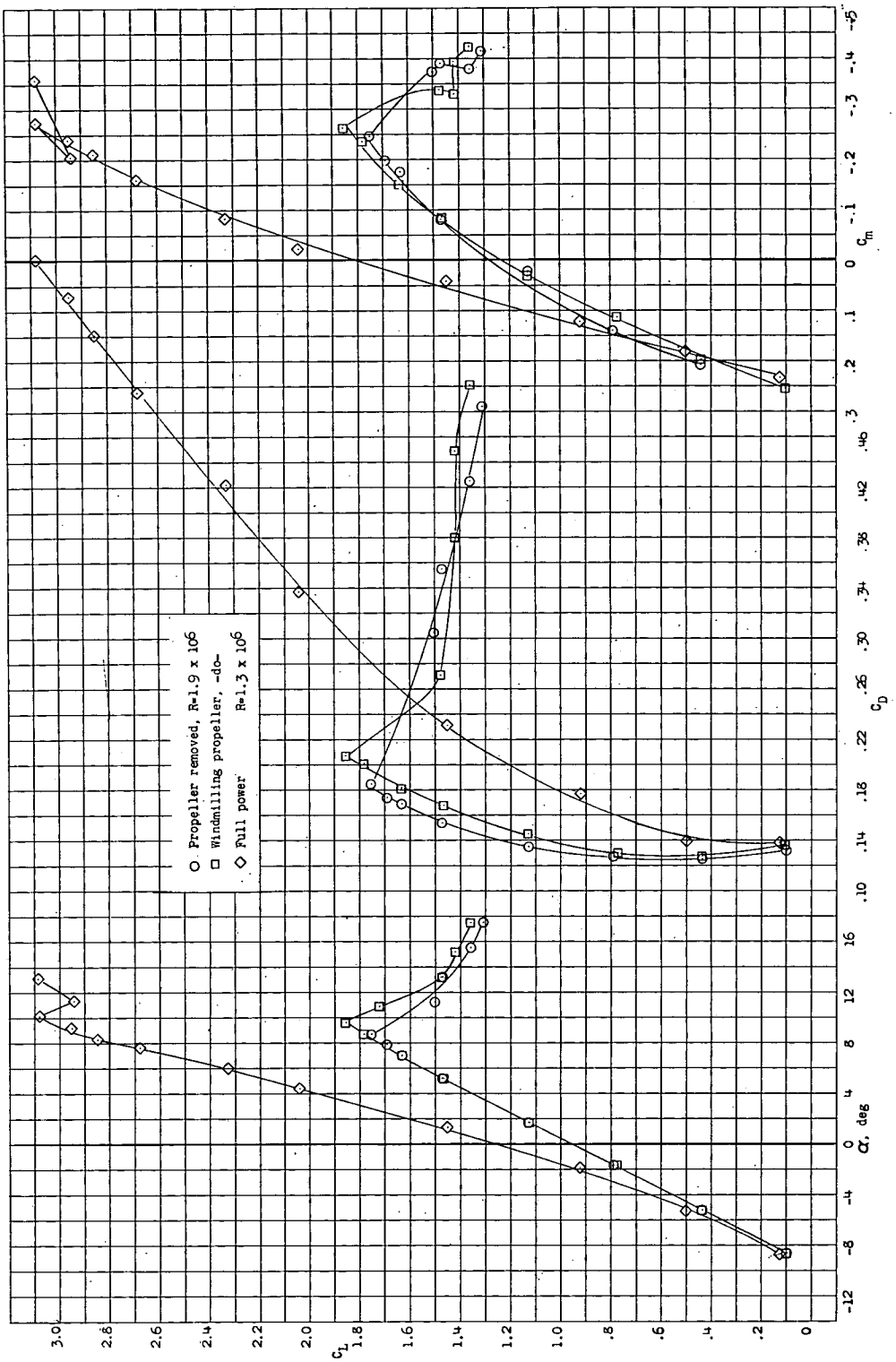


(b) Configuration B. Long nacelle; $C_{Q_S} = 0$; $C_{Q_B} = 0$.

Figure 6.- Continued.

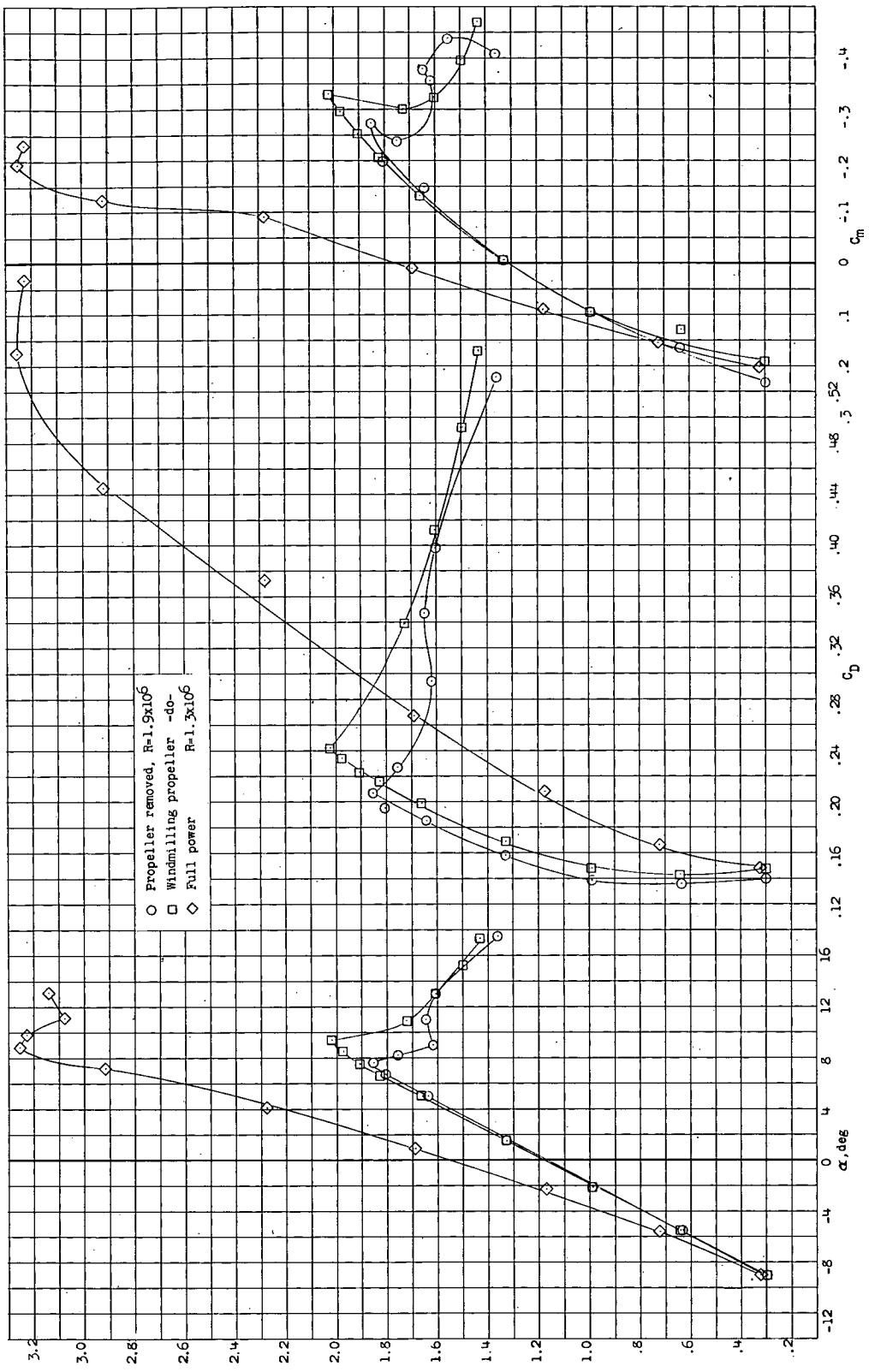


(c) Configuration C. Long nacelle; $C_{Q_S} = 0$; $C_{Q_B} = 0$.

Figure 6.- Continued.

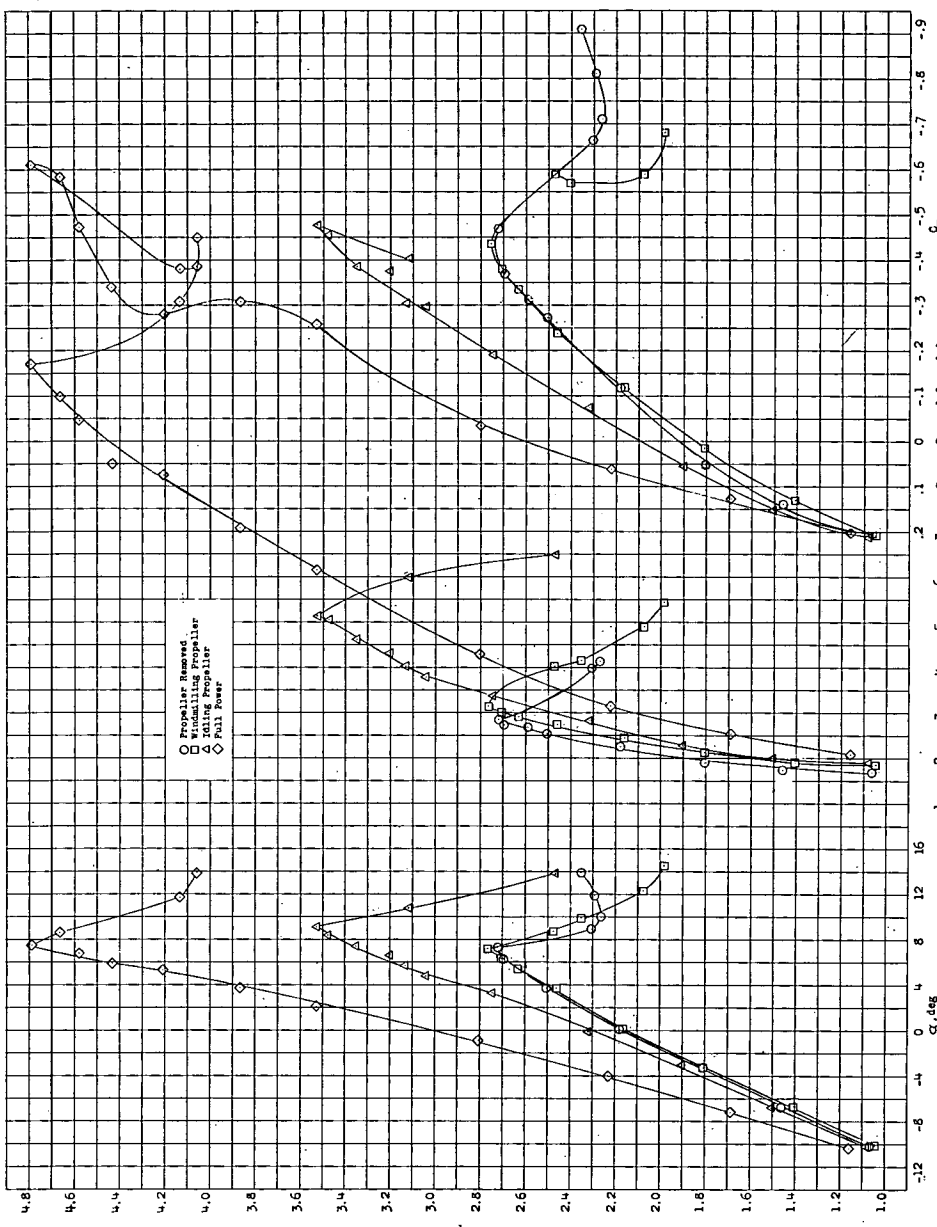


(d) Configuration D. Long nacelle; $C_{Q_S}$ = 0.035; $C_{Q_B}$ = 0.023;

R = 1.34 × $10^6$.

Figure 6.- Concluded.

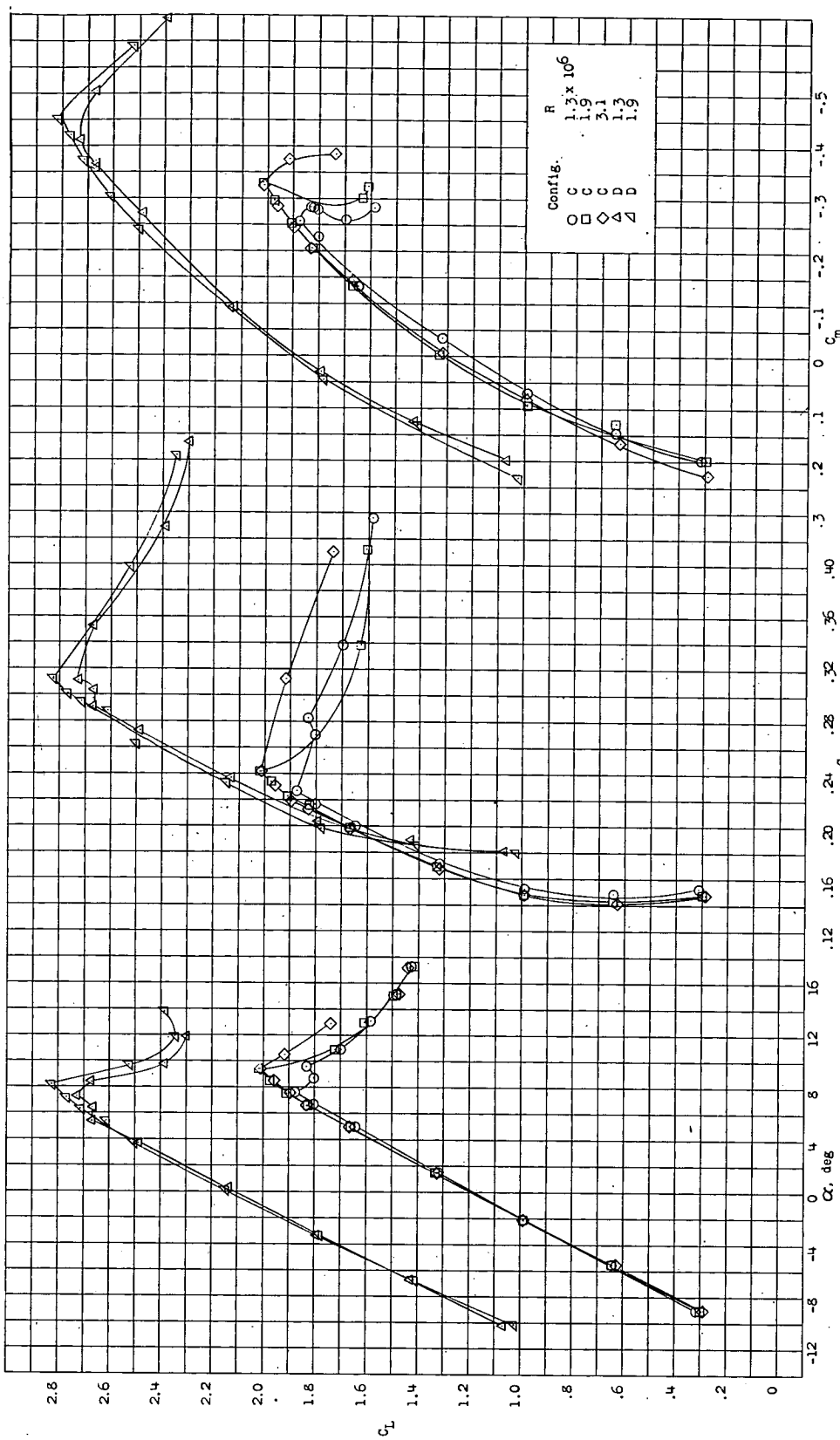


Figure 7.- Effect of Reynolds number on the longitudinal characteristics for configurations C and D.

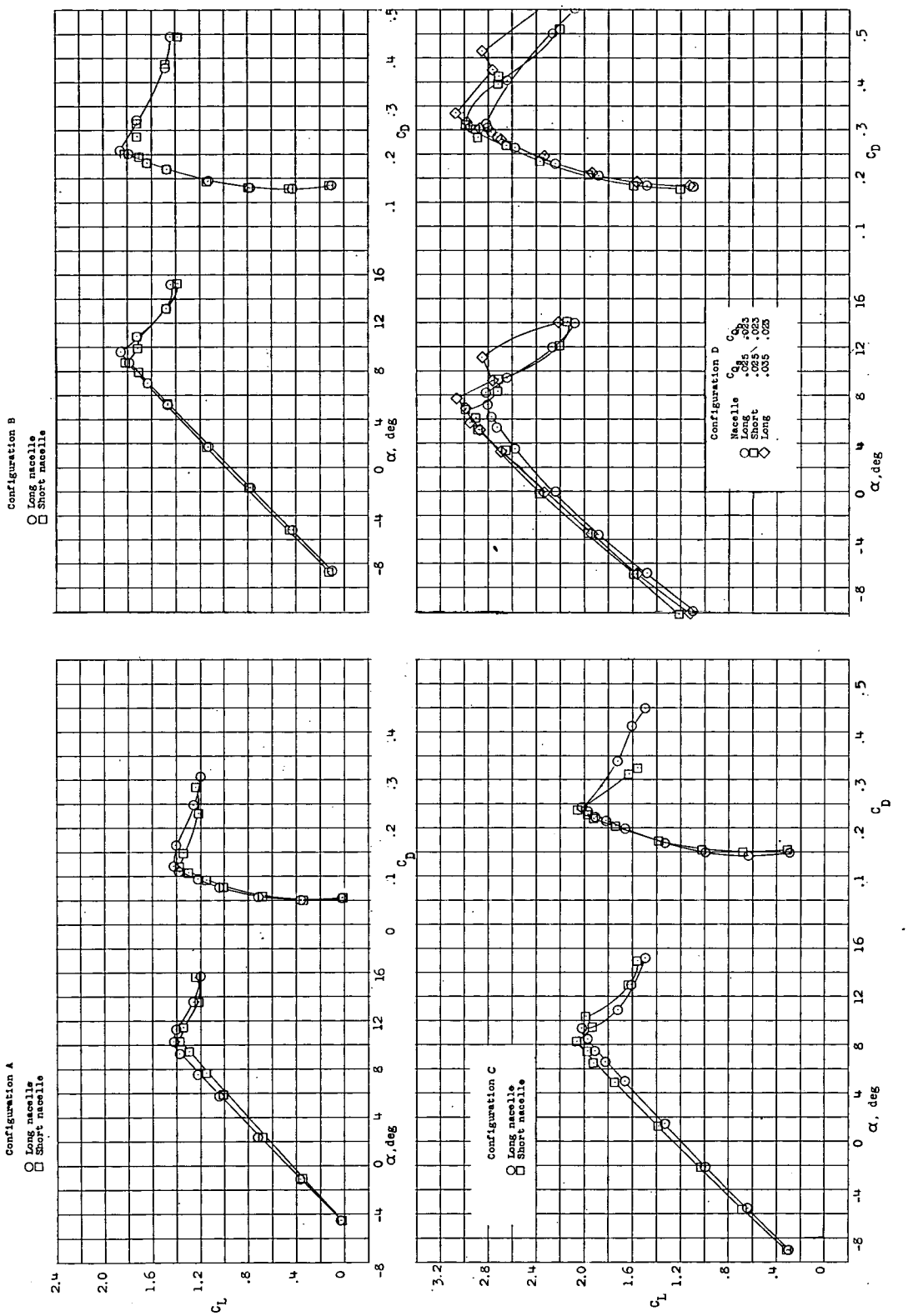


Figure 8.- Effect of nacelle length on the lift and drag characteristics.

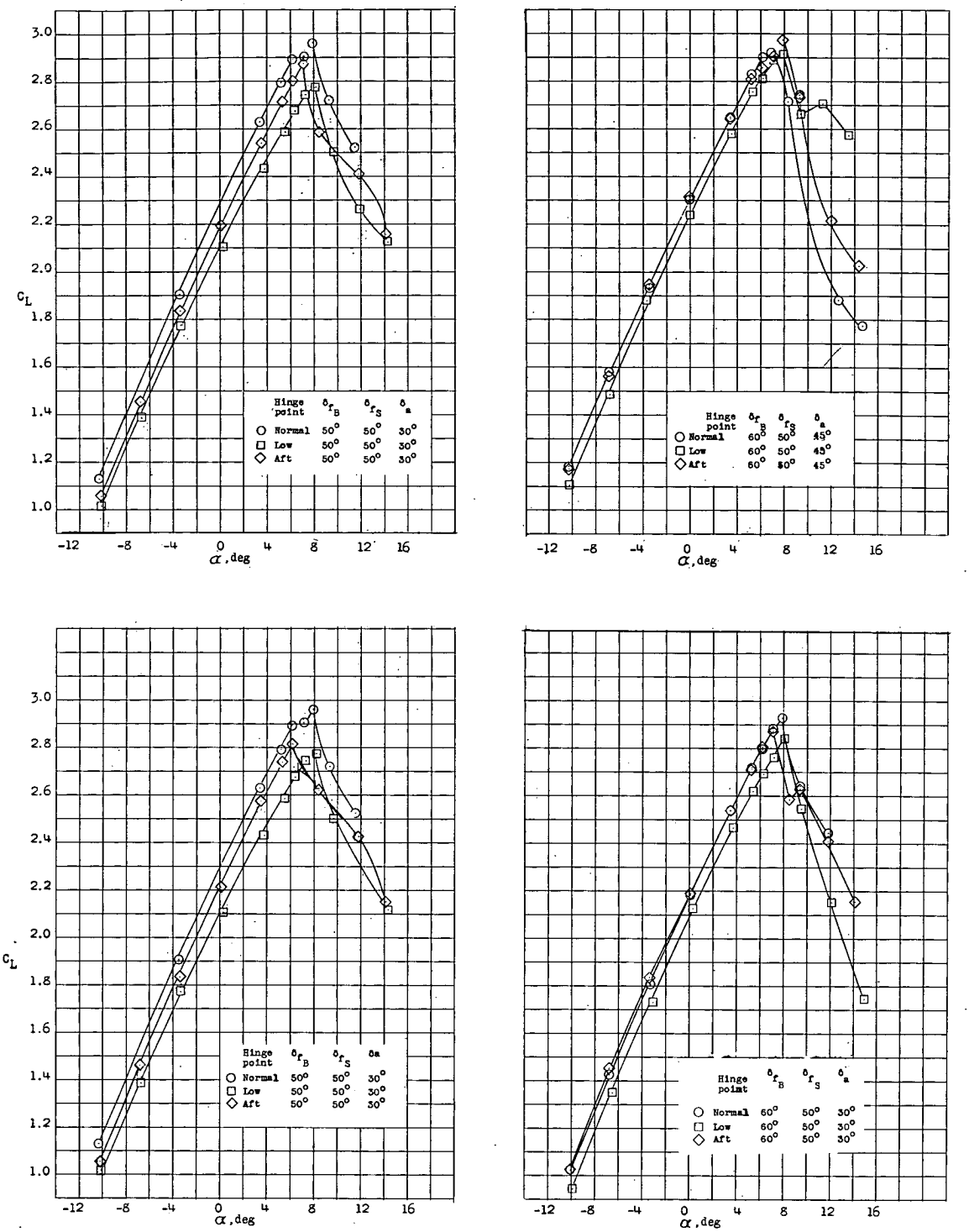


Figure 9.- The effect of blowing flap and aileron deflection and hinge position on the lift characteristics. $C_{Q_S}$ = 0.035; $C_{Q_B}$ = 0.023; windmilling propeller.

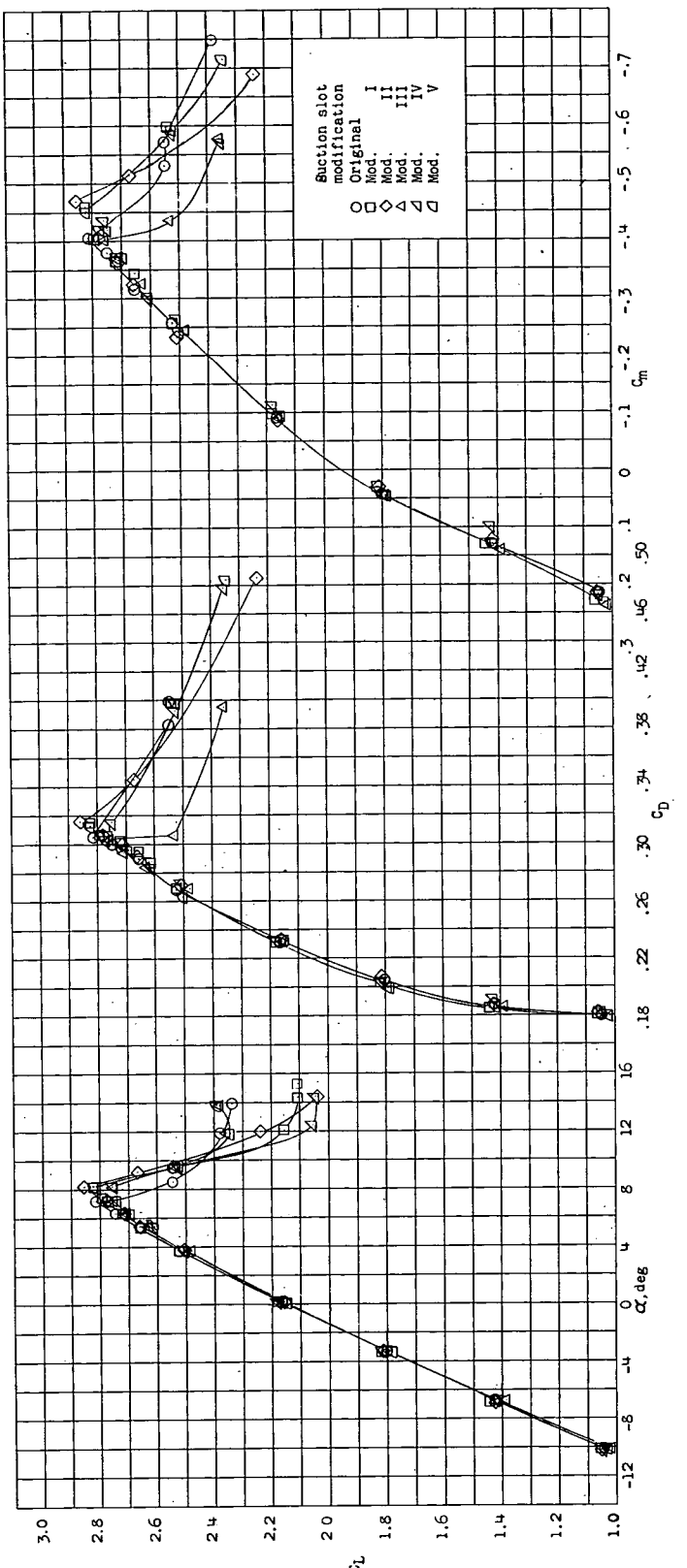


Figure 10.- Effect of suction slot configuration on the longitudinal characteristics. Model configuration D. $C_{Q_S}$ = 0.035; $C_{Q_B}$ = 0.023.

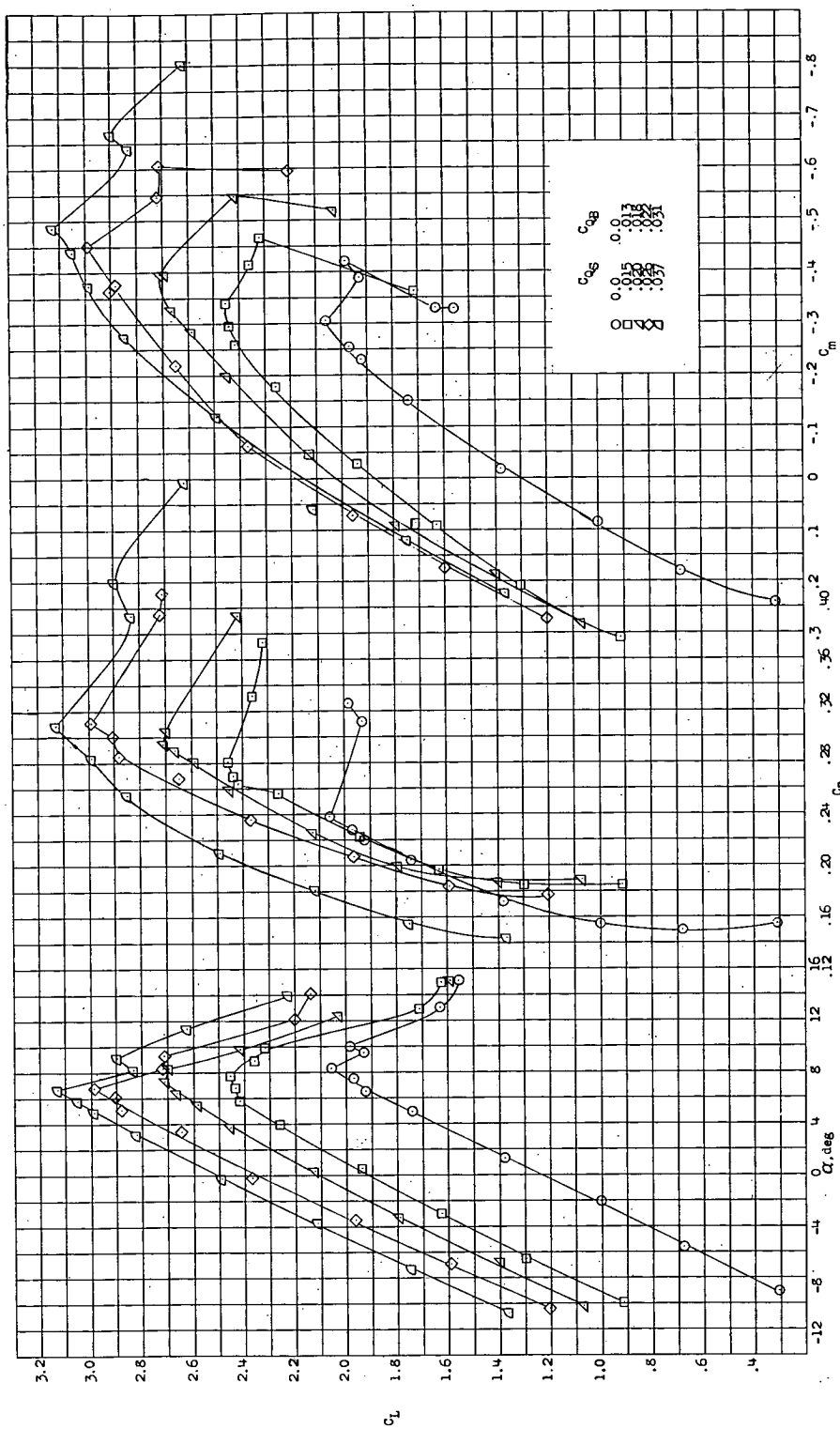


(a) Variation of $\alpha$, $C_D$, and $C_m$ with $C_L$ for equal quantities of suction and blowing.

Figure 11.- Effect of flow quantity variation on the longitudinal characteristics of the model with equal suction and blowing quantities. Configuration D. Short nacelle; windmilling propeller.

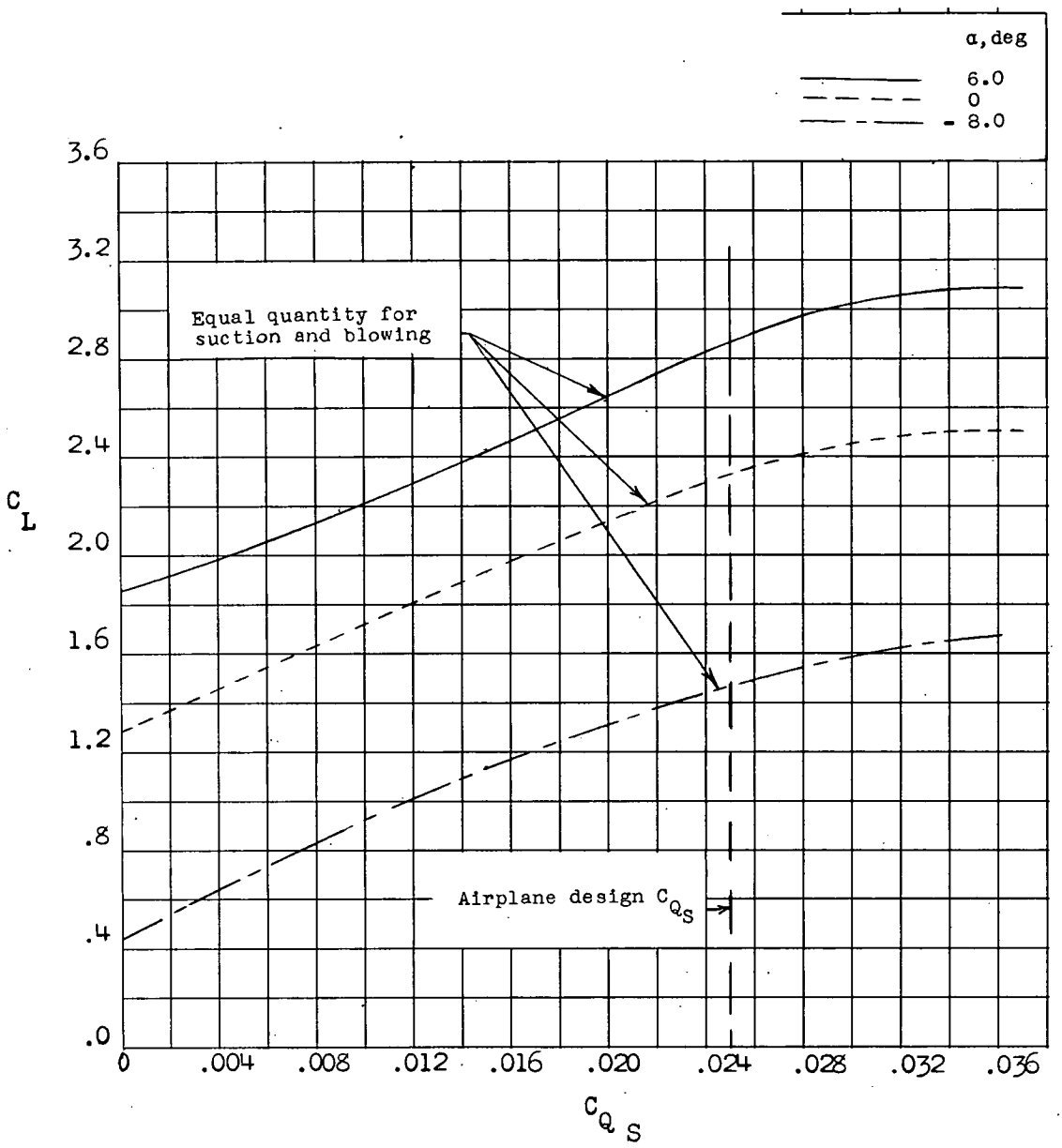


(b) Variation of lift coefficient with suction flow coefficient.

Figure 11.- Concluded.

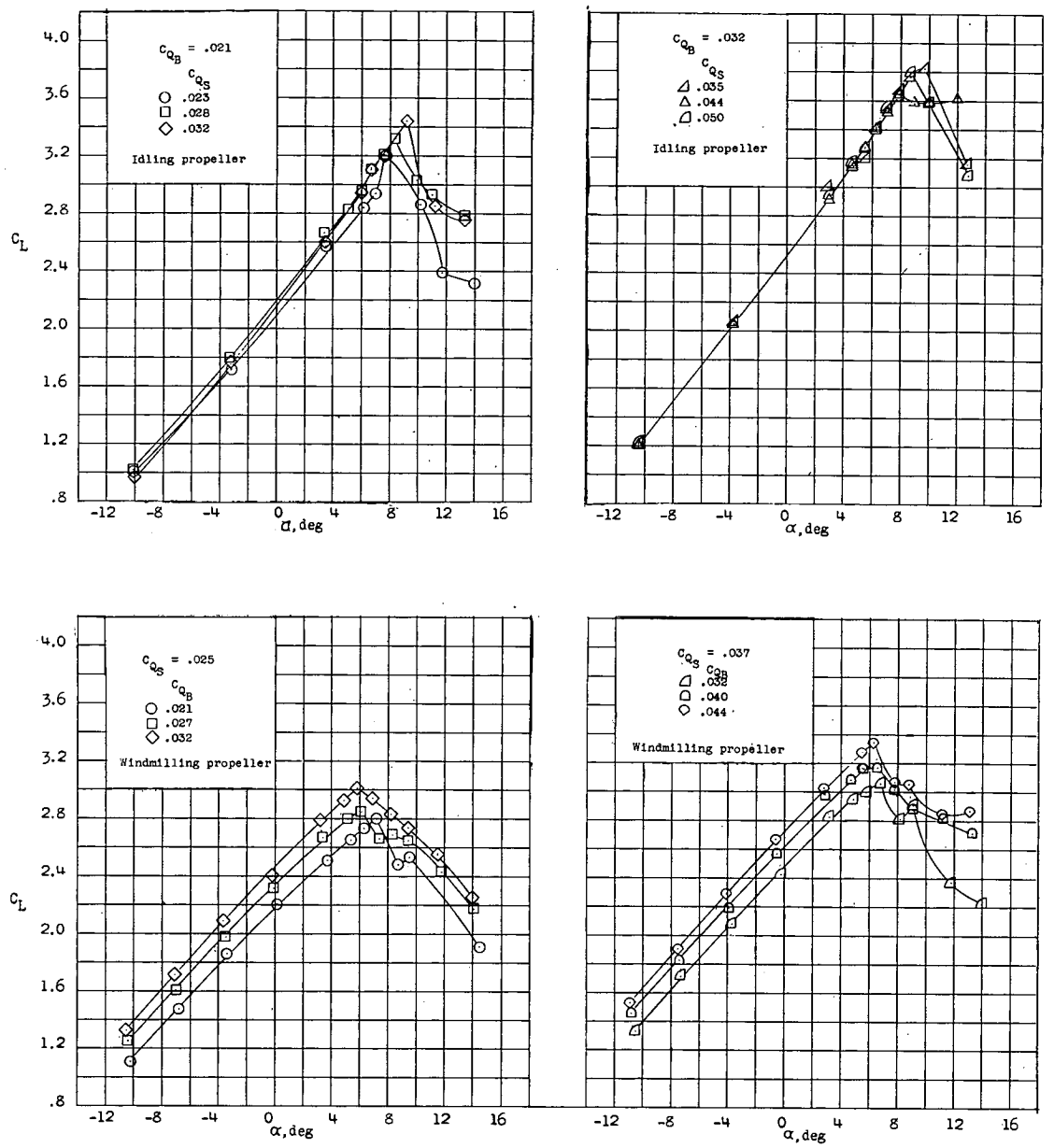


Figure 12.- Effect of independent variation of suction and blowing flow quantities. $R = 1.3 \times 10^6$.

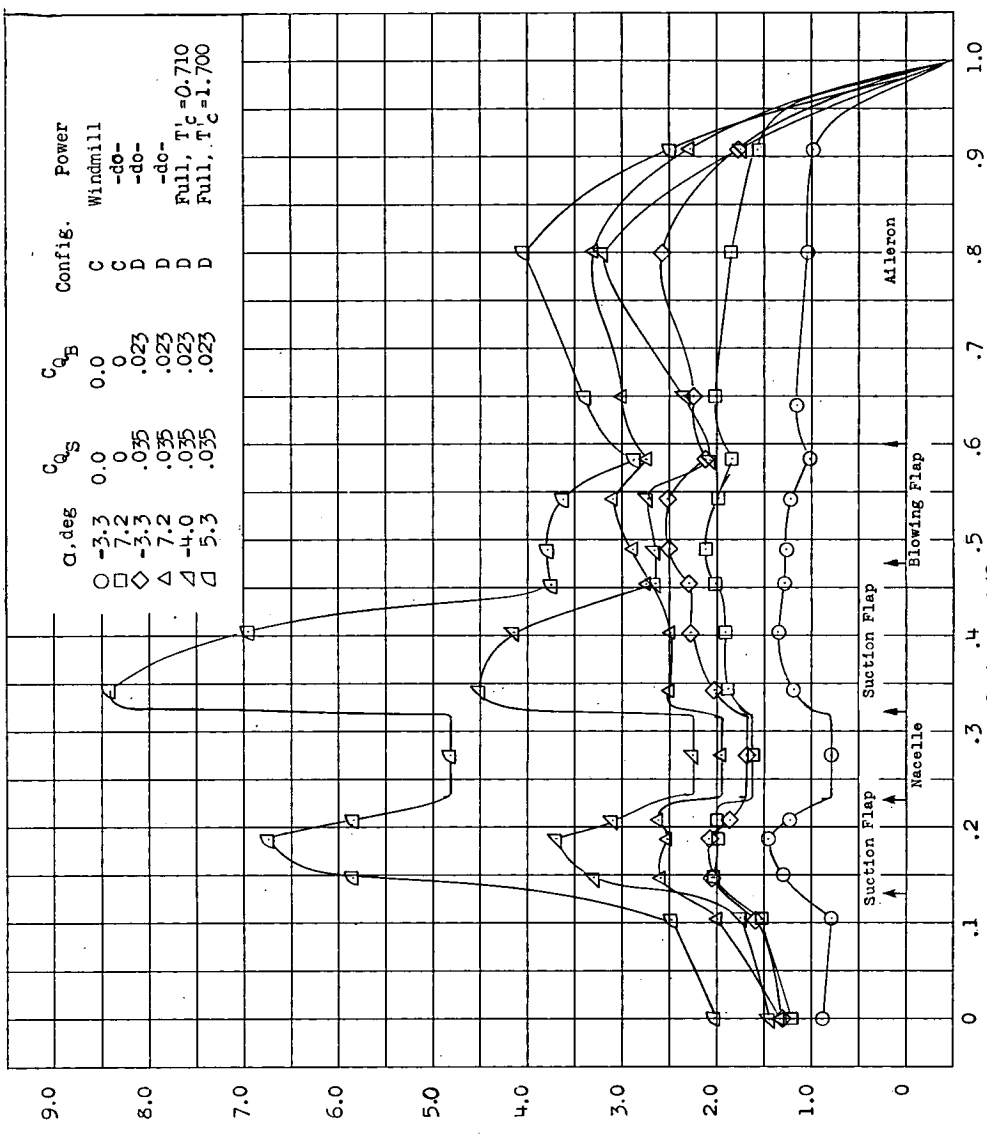


Figure 13.- Spanwise variation of section normal-force coefficient for the wing with and without boundary-layer control and propeller operation.

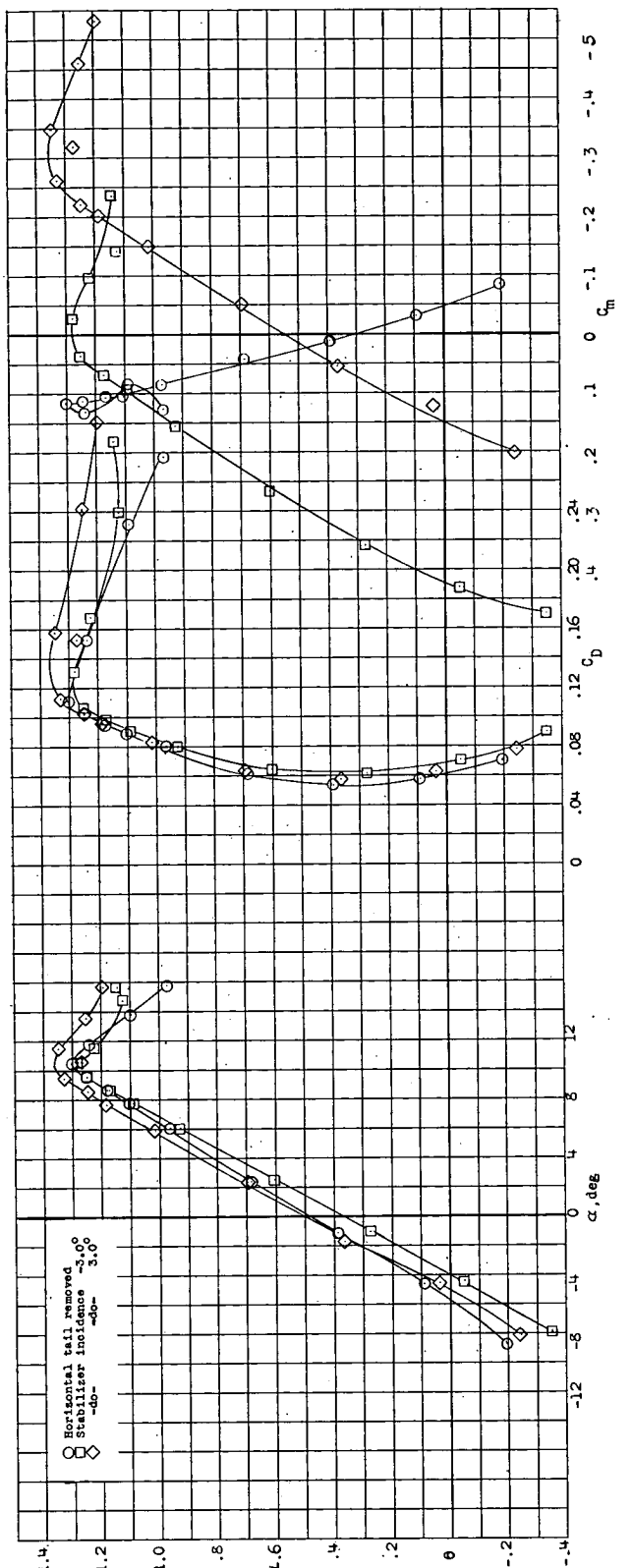


(a) Configuration A. Long nacelle; $C_{Q_S} = 0$; $C_{Q_B} = 0$; $R = 1.9 \times 10^6$; windmilling propeller.

Figure 14.- Longitudinal characteristics for four model configurations with tail incidence varied and with horizontal tail removed.

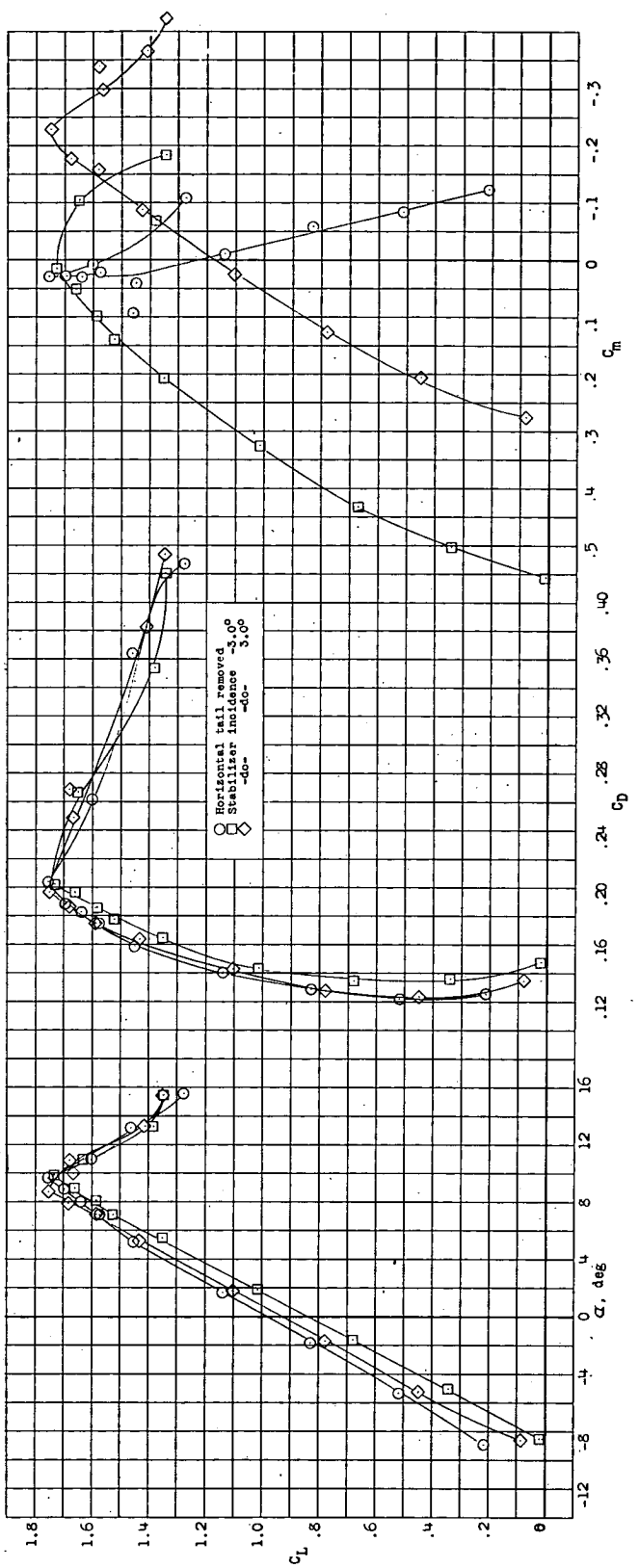


(b) Configuration B. Long nacelle; $C_{Q_S} = 0$; $C_{Q_B} = 0$; R = 1.9 × $10^6$; windmilling propeller.

Figure 14.- Continued.

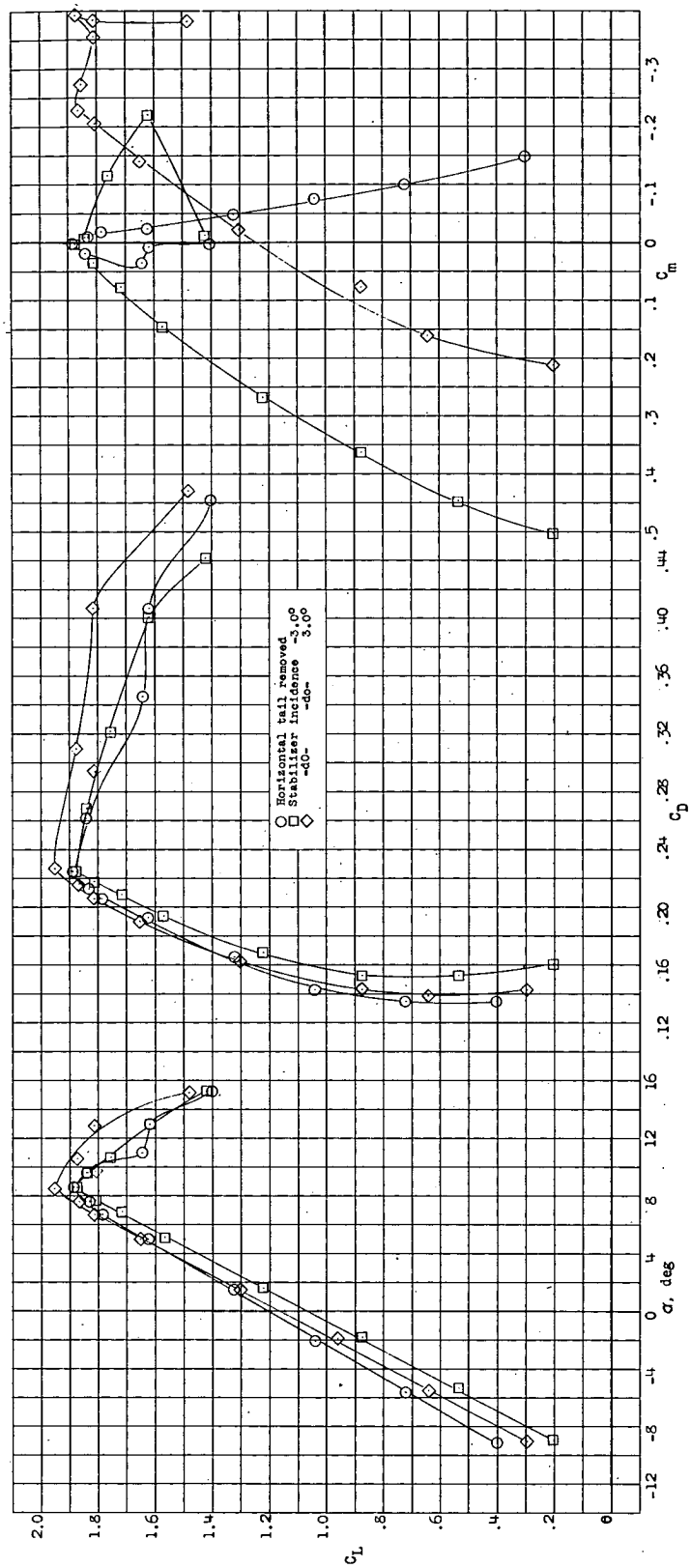


(c) Configuration C. Long nacelle; $C_{Q_S} = 0$; $C_{Q_B} = 0$; R = 1.9 × $10^6$; windmilling propeller.

Figure 14.- Continued.

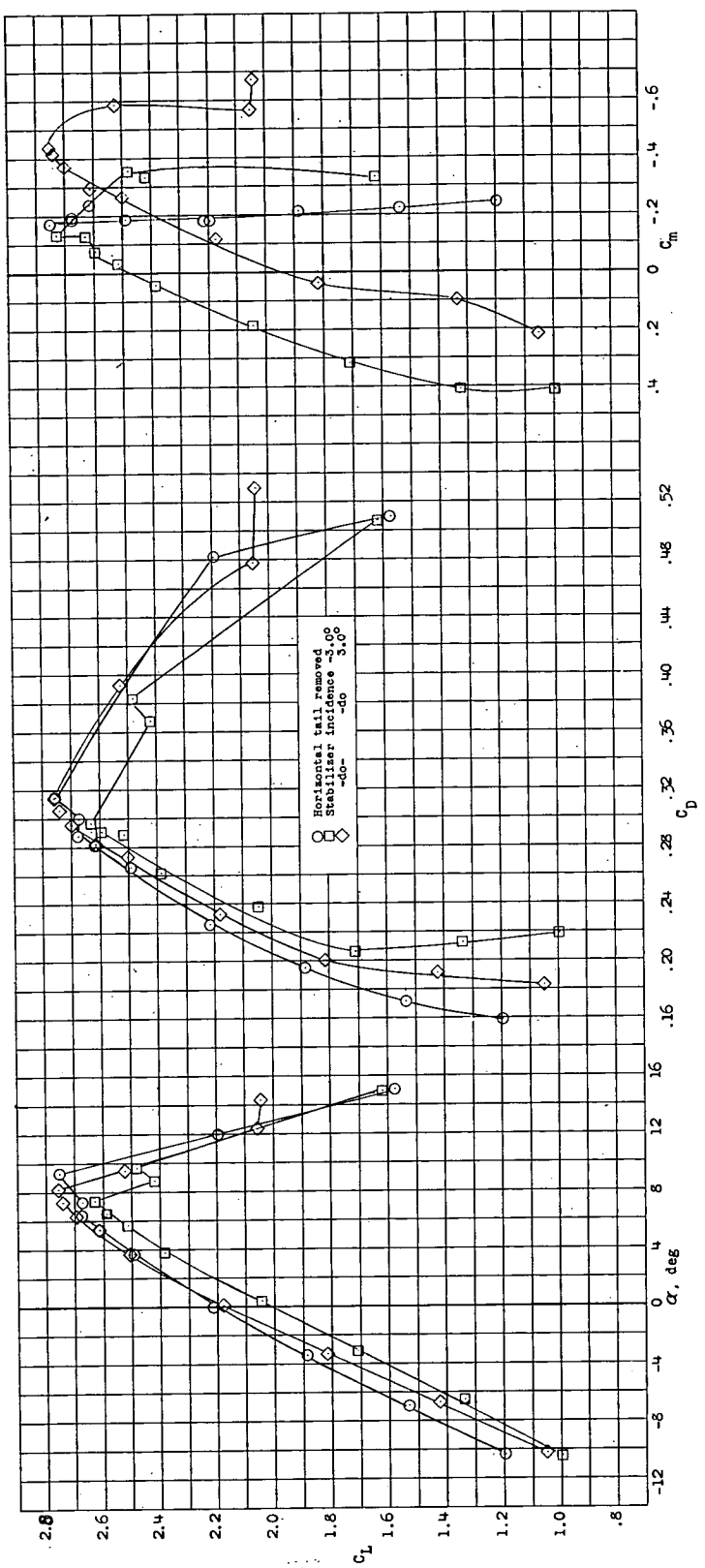


(d) Configuration D. Long nacelle; $C_{Q_S}$ = 0.035; $C_{Q_B}$ = 0.023; R = 1.9 × $10^6$; windmilling propeller.

Figure 14.- Continued.

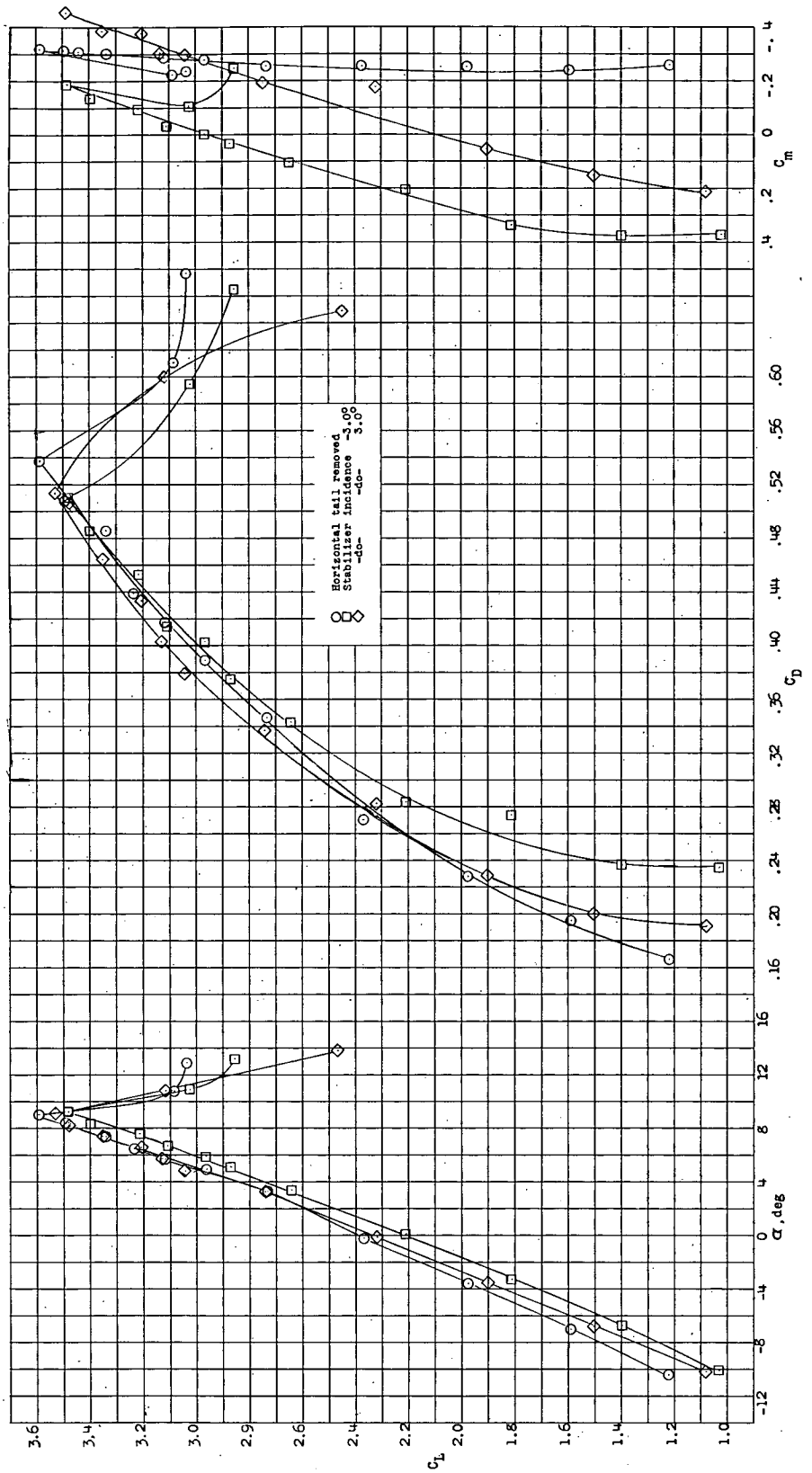


(e) Configuration D. Long nacelle; $C_{Q_S}$ = 0.035; $C_{Q_B}$ = 0.023; R = 1.34 × $10^6$; idling propellers.

Figure 14.- Continued.

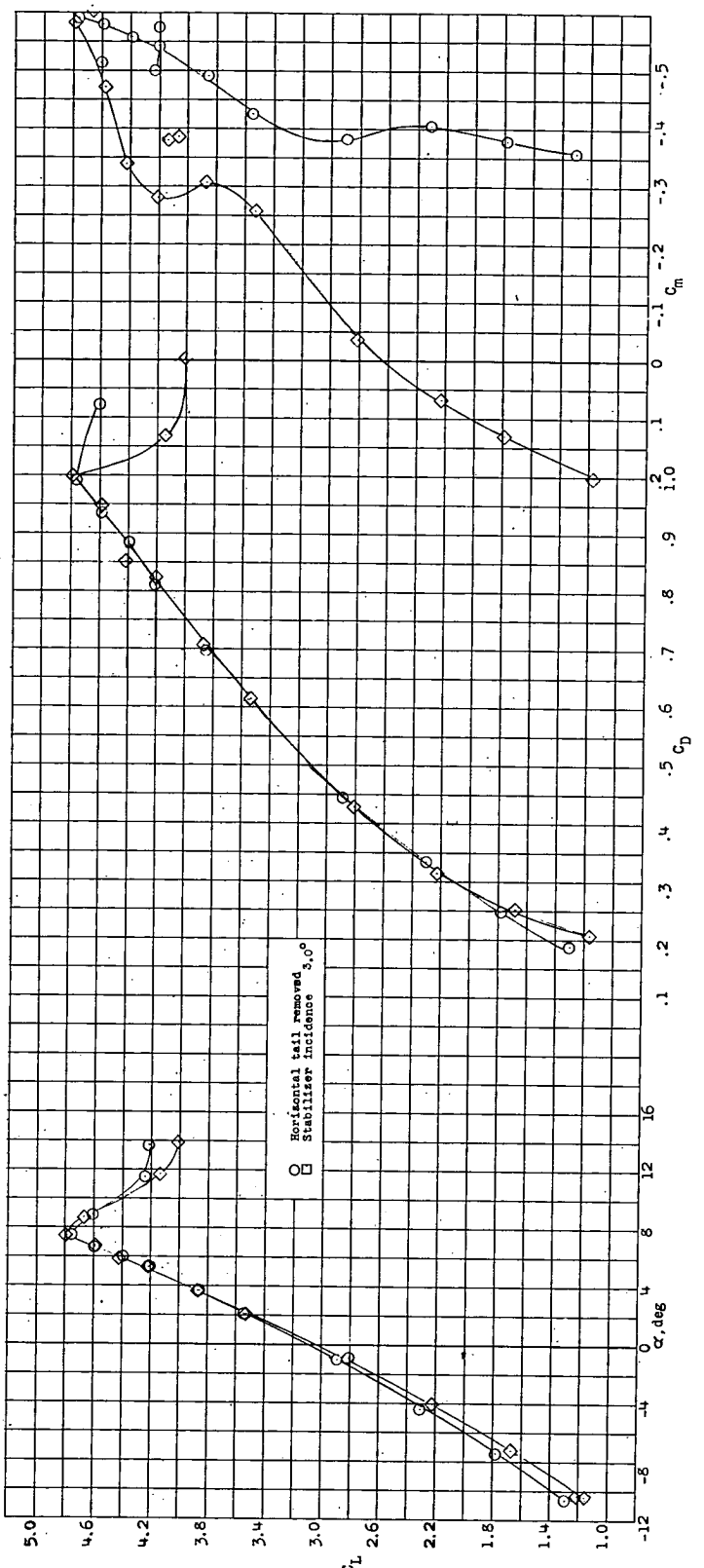


(f) Configuration D. Long nacelle; $C_{Q_S}$ = 0.035; $C_{Q_B}$ = 0.023; R = 1.34 × 10⁶; full power.

Figure 14.- Concluded.

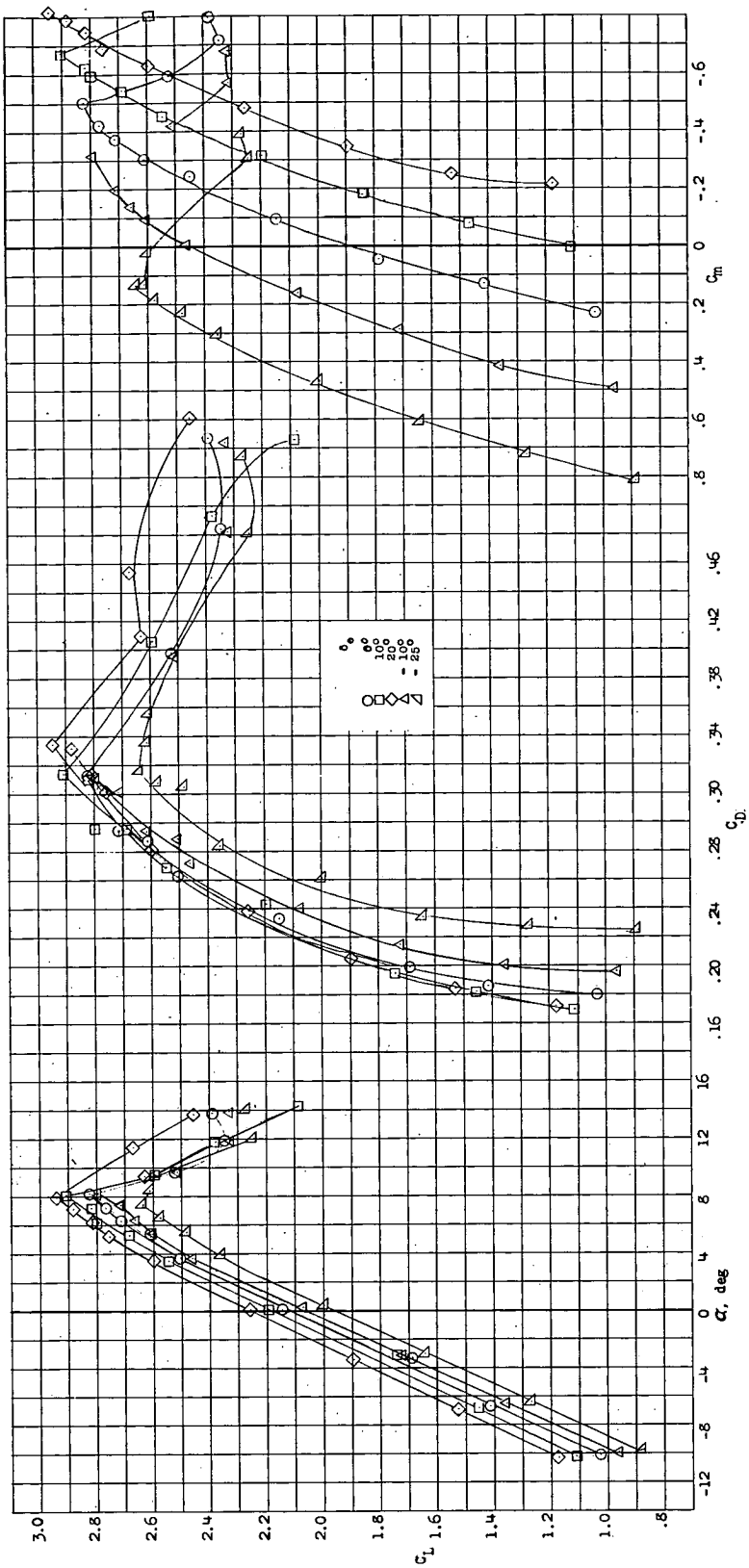


(a) Configuration D. Long nacelle; $C_{Q_S}$ = 0.035; $C_{Q_B}$ = 0.023; R = 1.9 × $10^6$; windmilling propeller.

Figure 15.- Effect of elevator deflection on the longitudinal characteristics of the model.

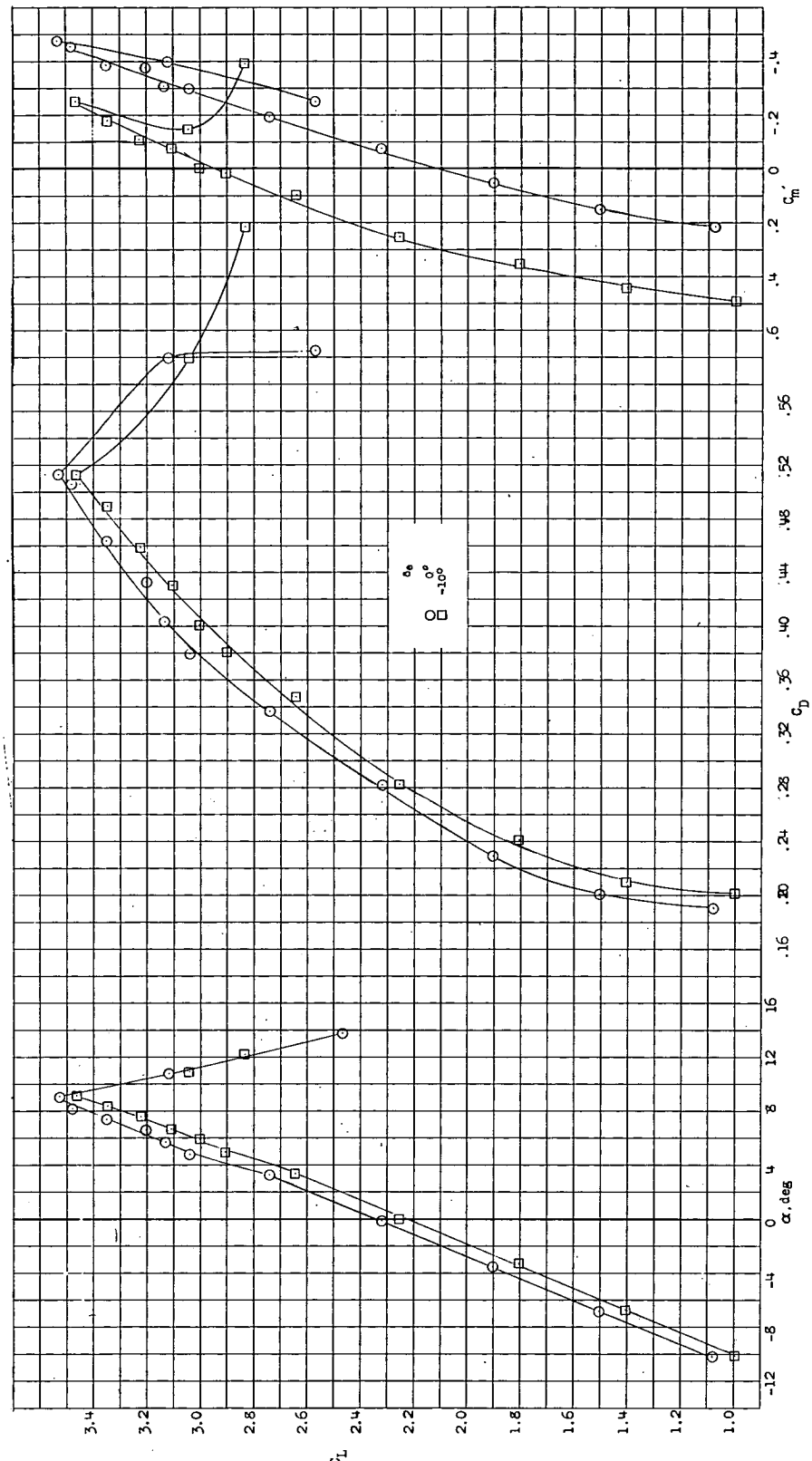


(b) Configuration D. Long nacelle; $C_{Q_S}$ = 0.035; $C_{Q_B}$ = 0.023; R = 1.34 × $10^6$; idling propellers.

Figure 15.- Continued.

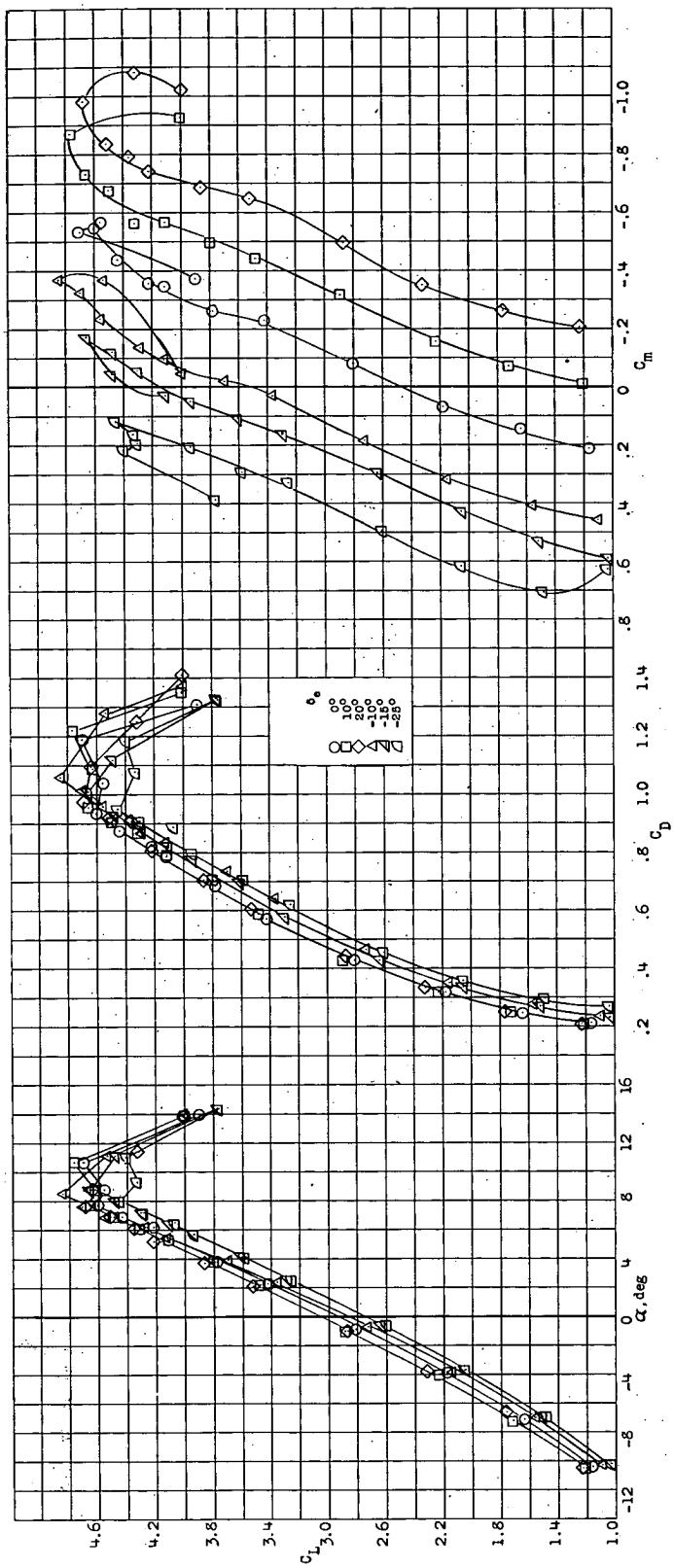


(c) Configuration D. Long nacelle; $C_{Q_S}$ = 0.035; $C_{Q_B}$ = 0.023; R = 1.34 × $10^6$; full power.

Figure 15.- Concluded.

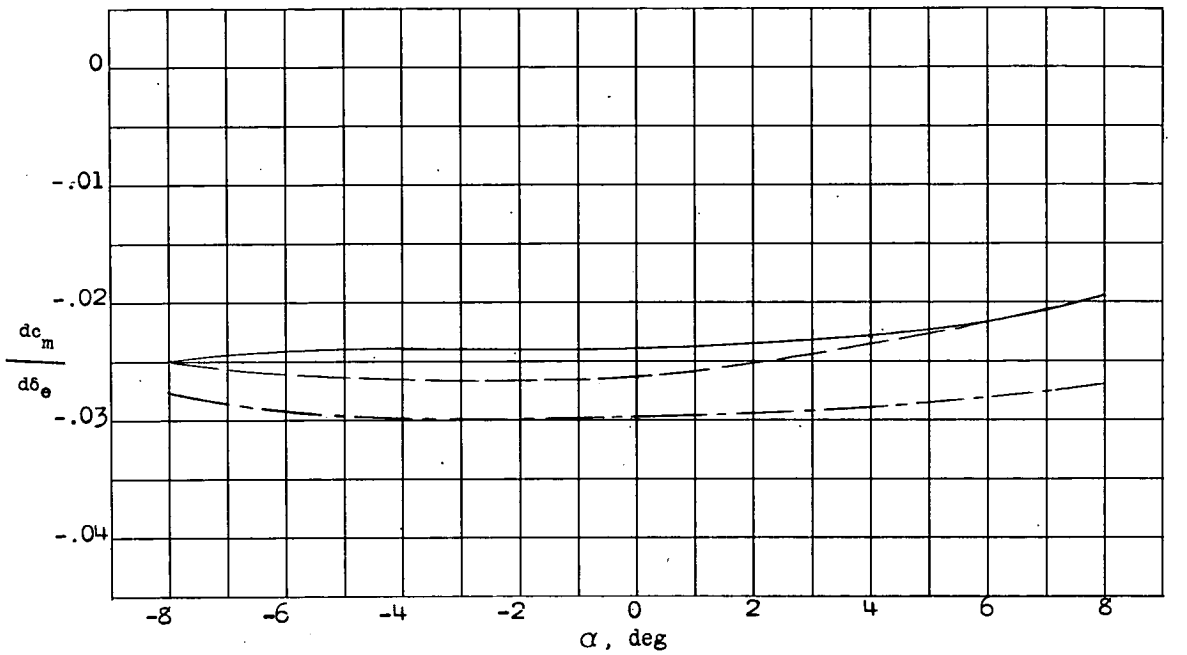


(a) Elevator effectiveness.

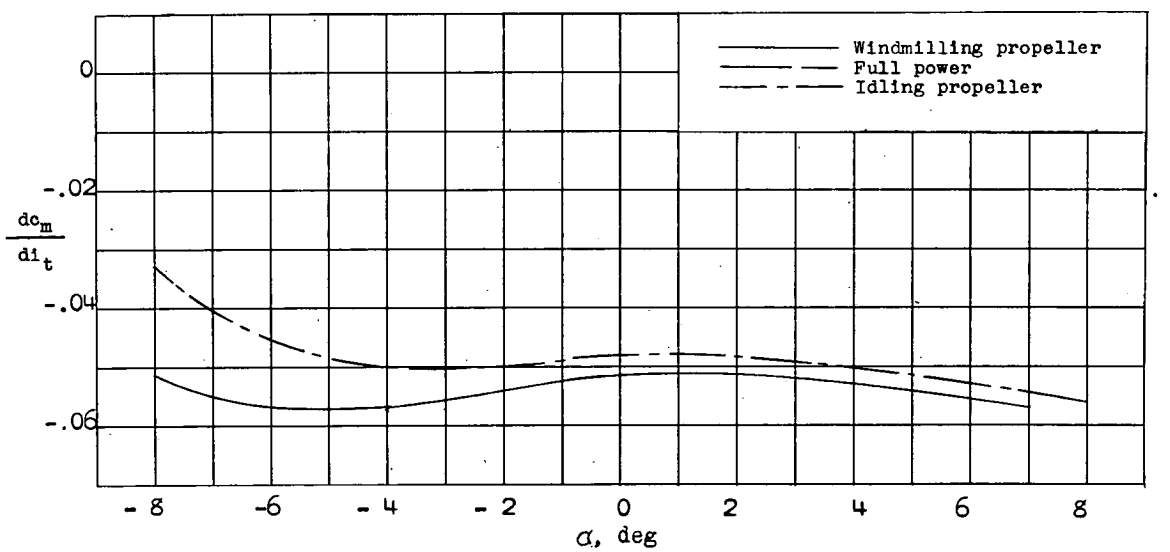


(b) Stabilizer effectiveness.

Figure 16.- Variation of horizontal tail effectiveness parameters with angle of attack.

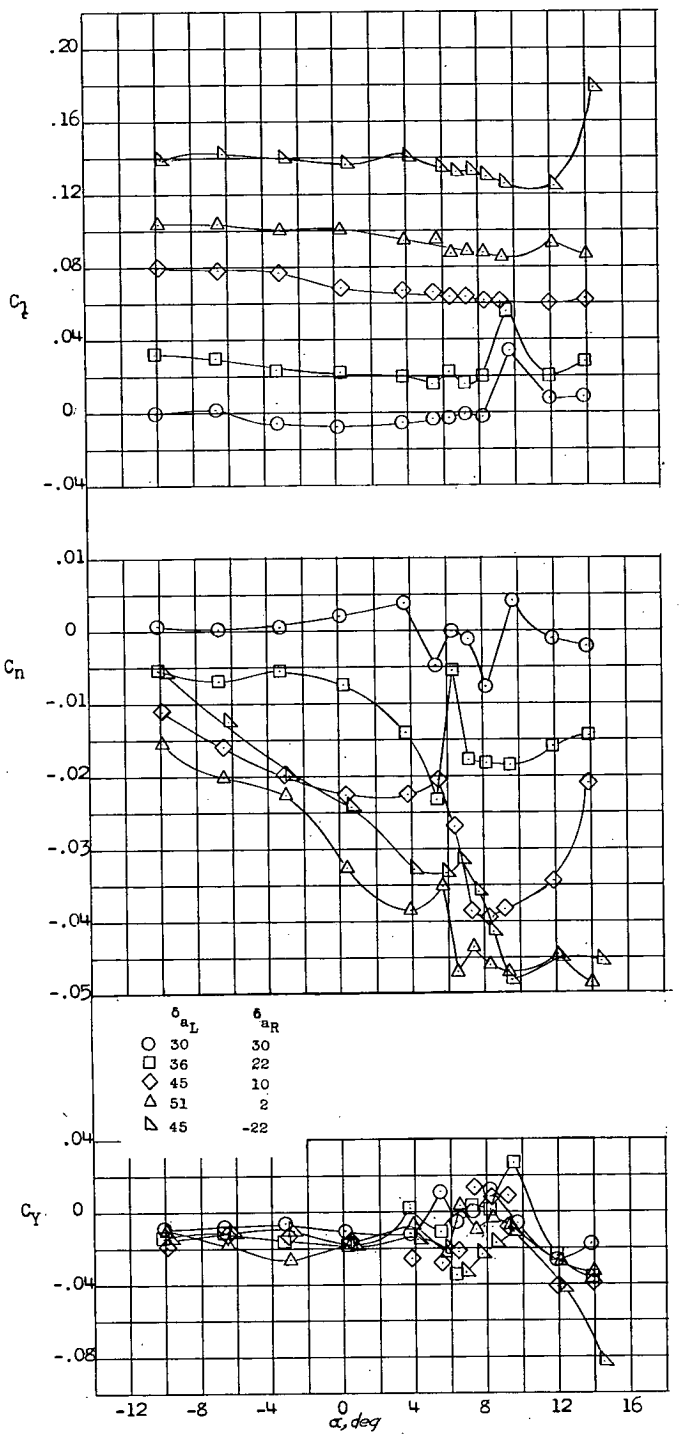


(a) Variation of $C_l$, $C_n$, and $C_Y$ with angle of attack for windmilling propeller.

Figure 17.- Effect of aileron deflection on the aerodynamic characteristics for $\psi = 0^\circ$.

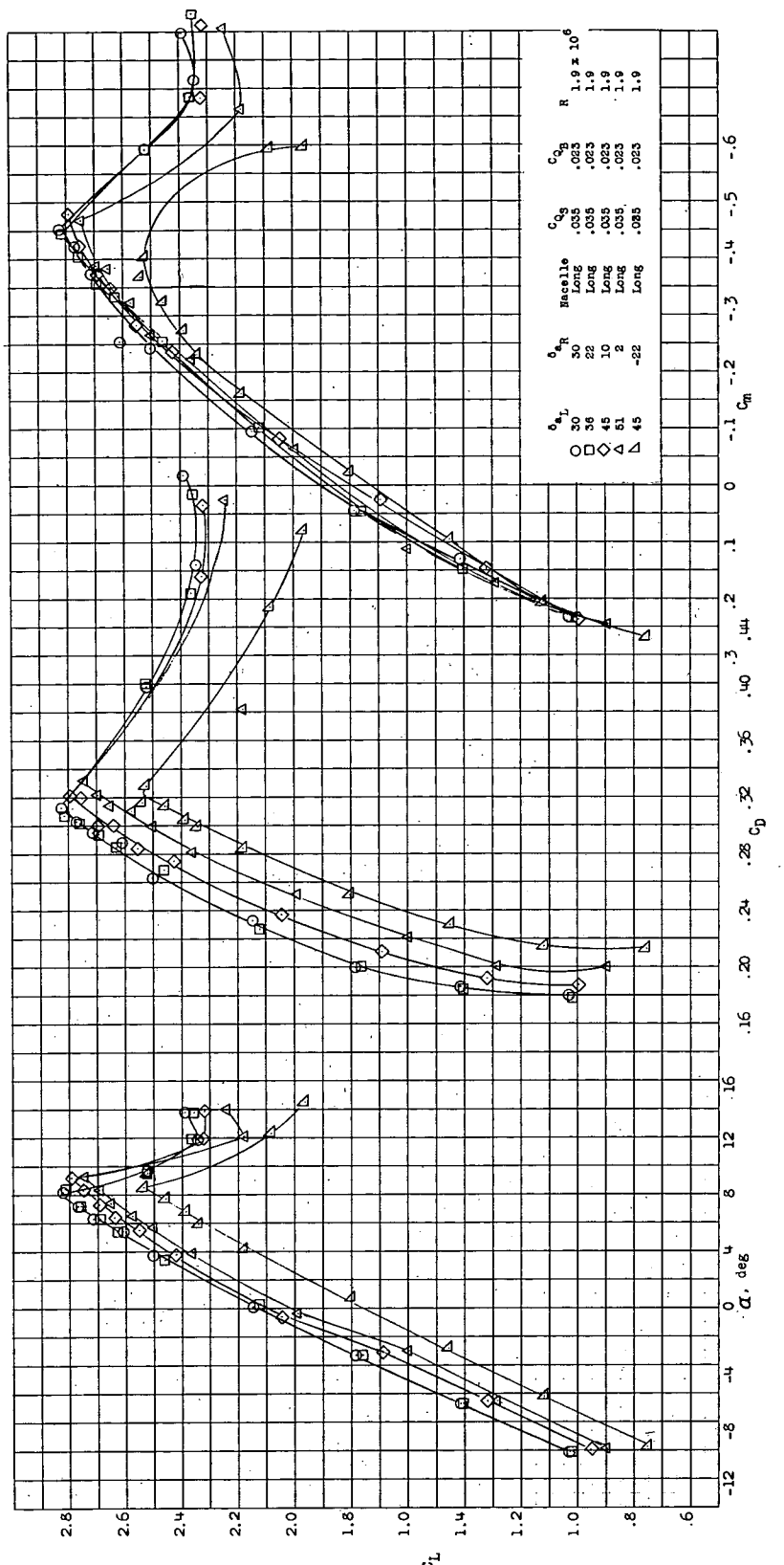


(a) Concluded. Variation of $\alpha$, $C_D$, and $C_m$ with $C_L$ for windmilling propeller.

Figure 17.- Continued.

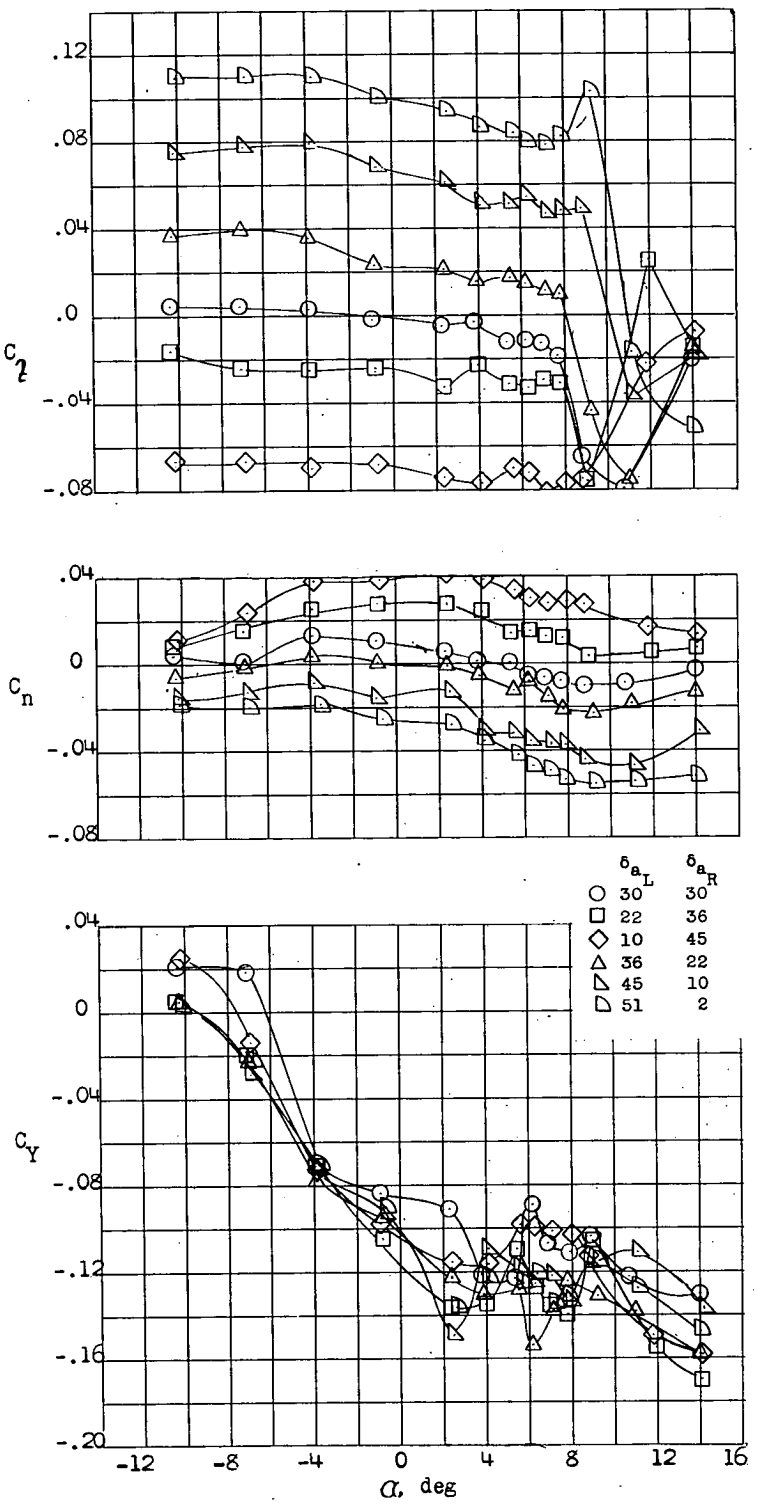


(b) Variation of $C_l$, $C_n$, and $C_Y$ with angle of attack for full power.

Figure 17.- Continued.

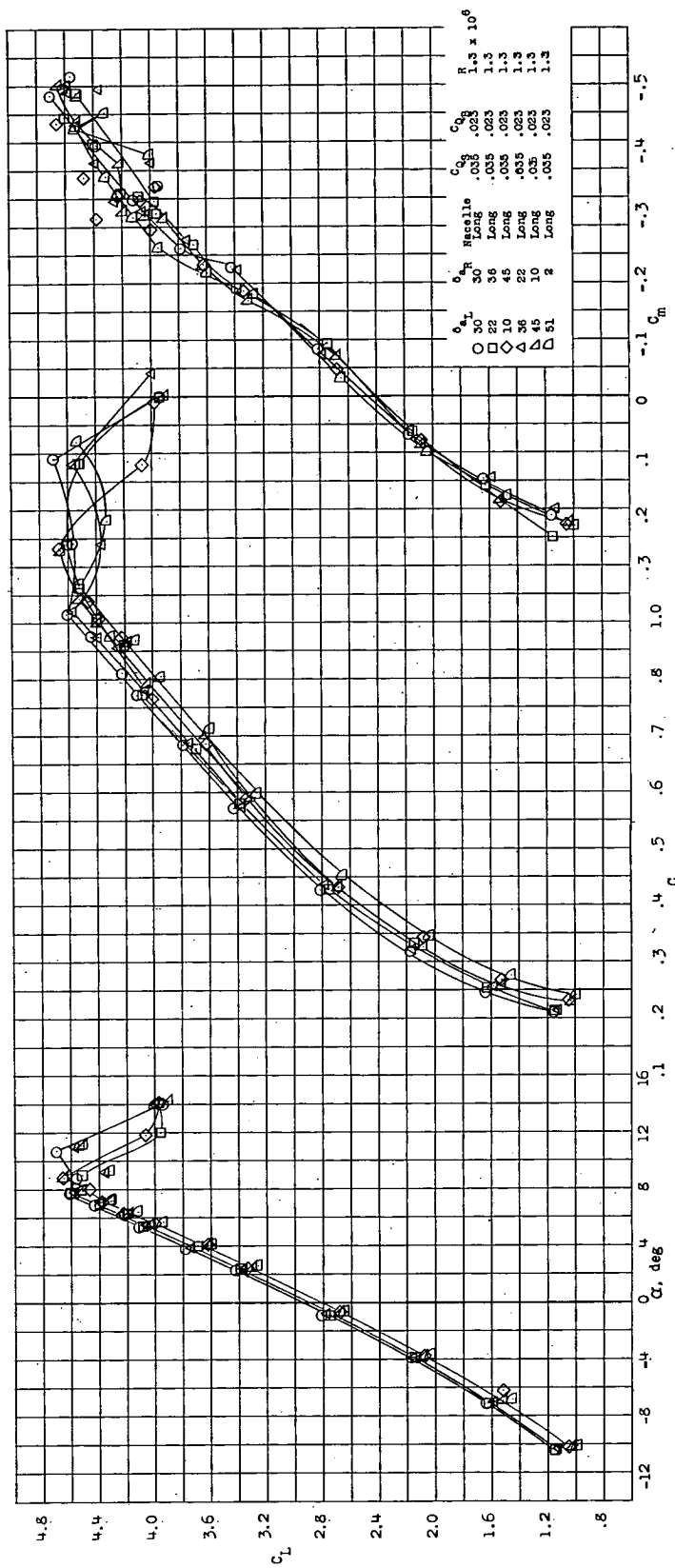


(b) Concluded. Variation of $\alpha$, $C_D$, and $C_m$ with $C_L$ for full power.

Figure 17.- Continued.

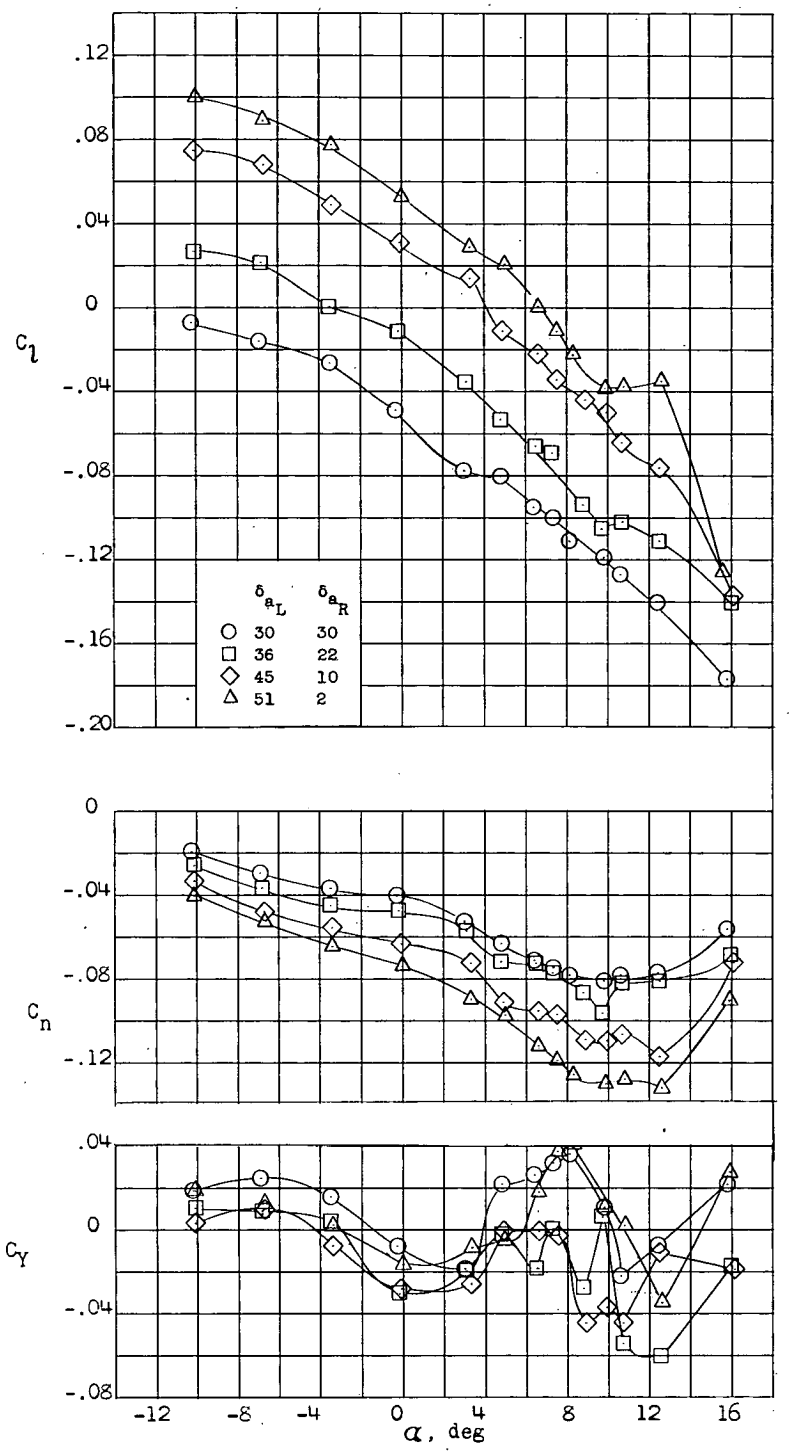


(c) Variation of $C_l$, $C_n$, and $C_Y$ with angle of attack for asymmetric power. (Full power on right side.)

Figure 17.- Continued.

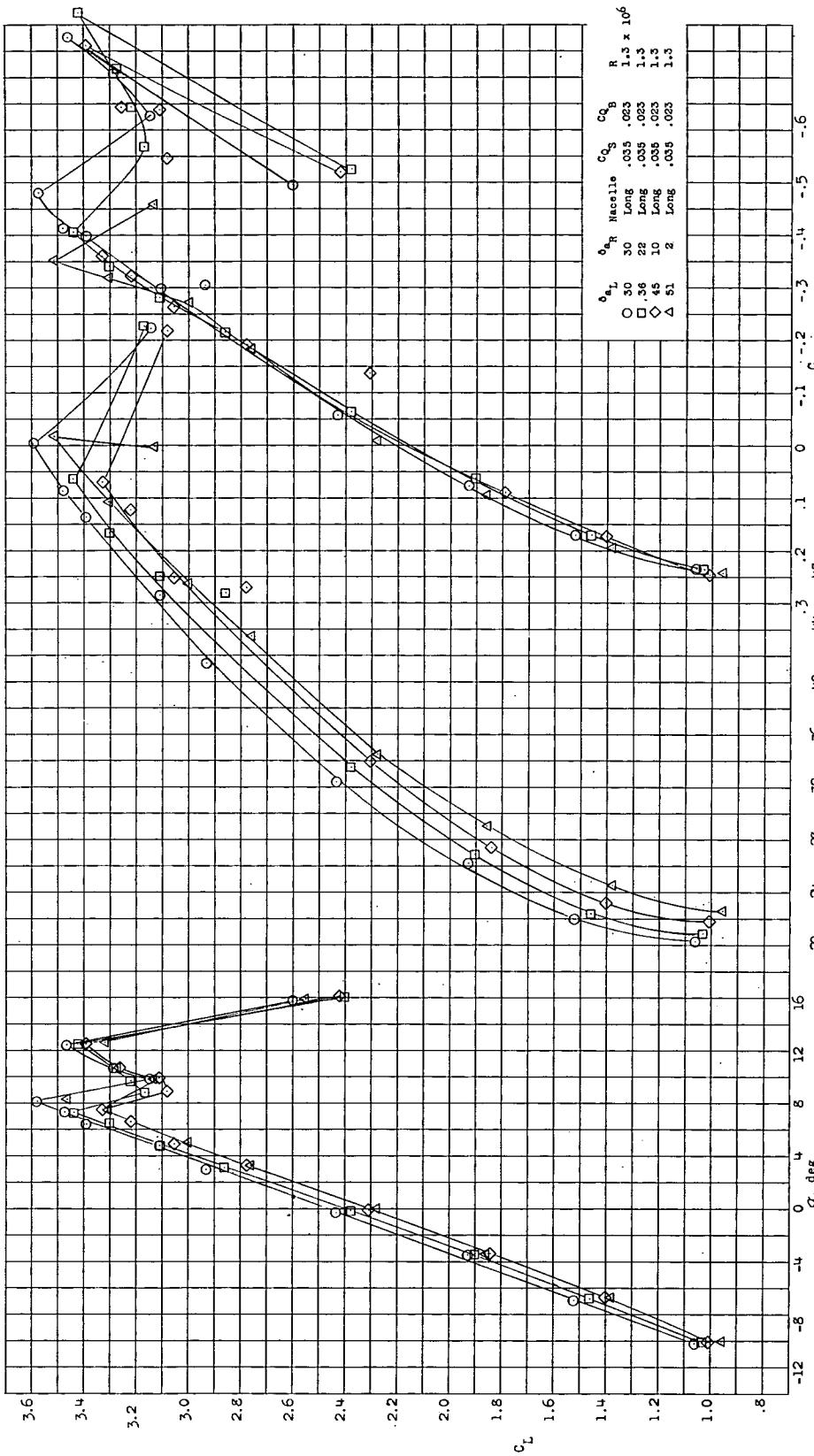


(c) Concluded. Variation of $\alpha$, $C_D$, and $C_m$ with $C_L$ for asymmetric power. (Full power on right side.)

Figure 17.- Continued.

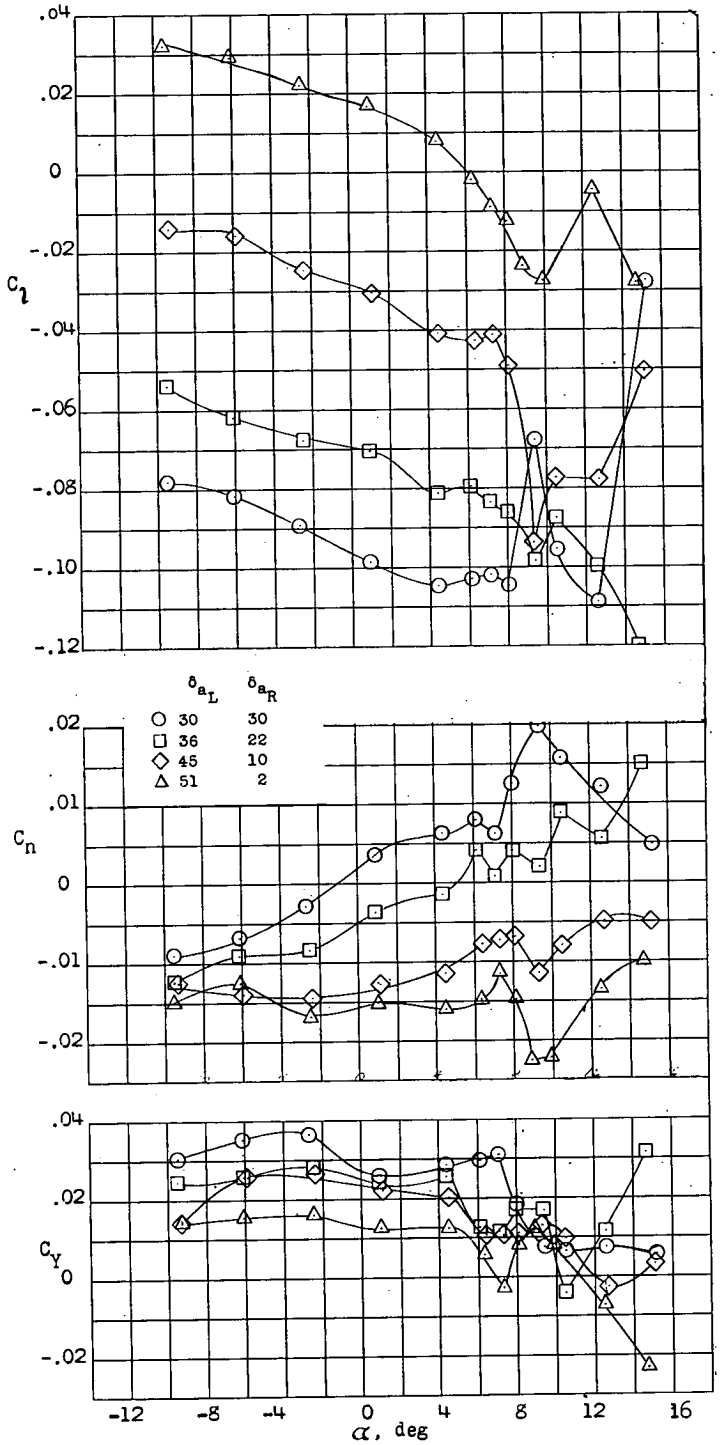


(d) Variation of $C_l$, $C_n$, and $C_Y$ with angle of attack for asymmetric boundary-layer control. (Left side off.)

Figure 17.- Continued.

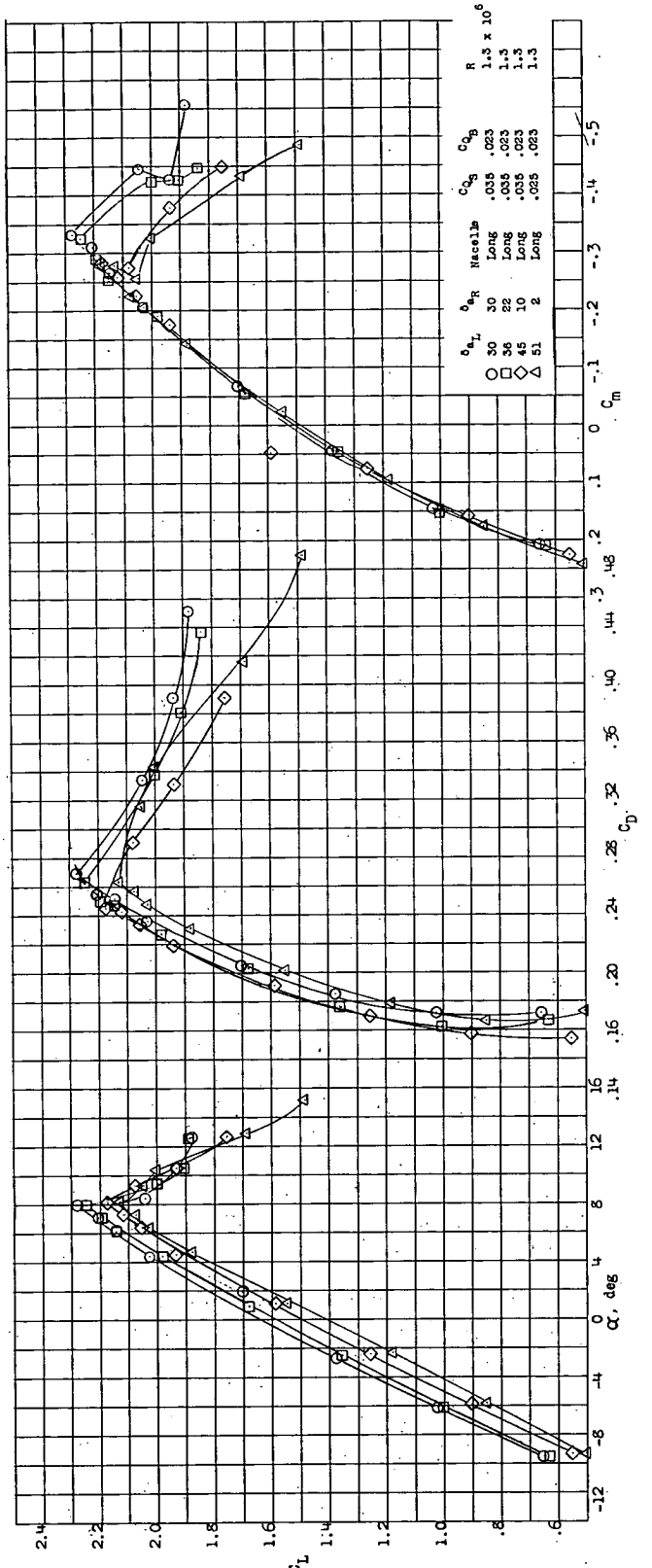


(d) Concluded. Variation of $\alpha$, $C_D$, and $C_m$ with $C_L$ for asymmetric boundary-layer control. (Left side off.)

Figure 17.- Concluded.

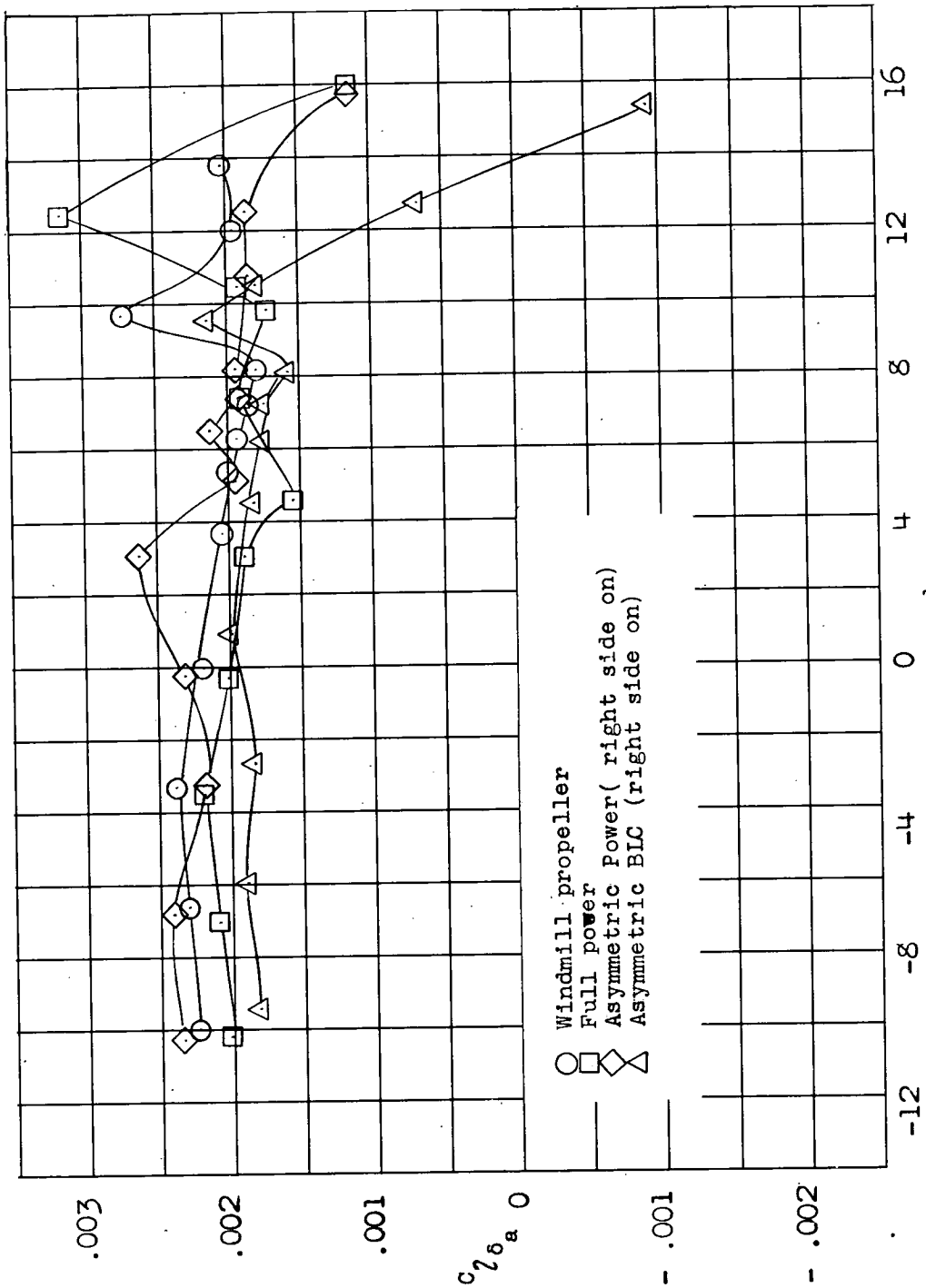


Figure 18.- Variation of aileron effectiveness parameter with angle of attack for several power conditions.

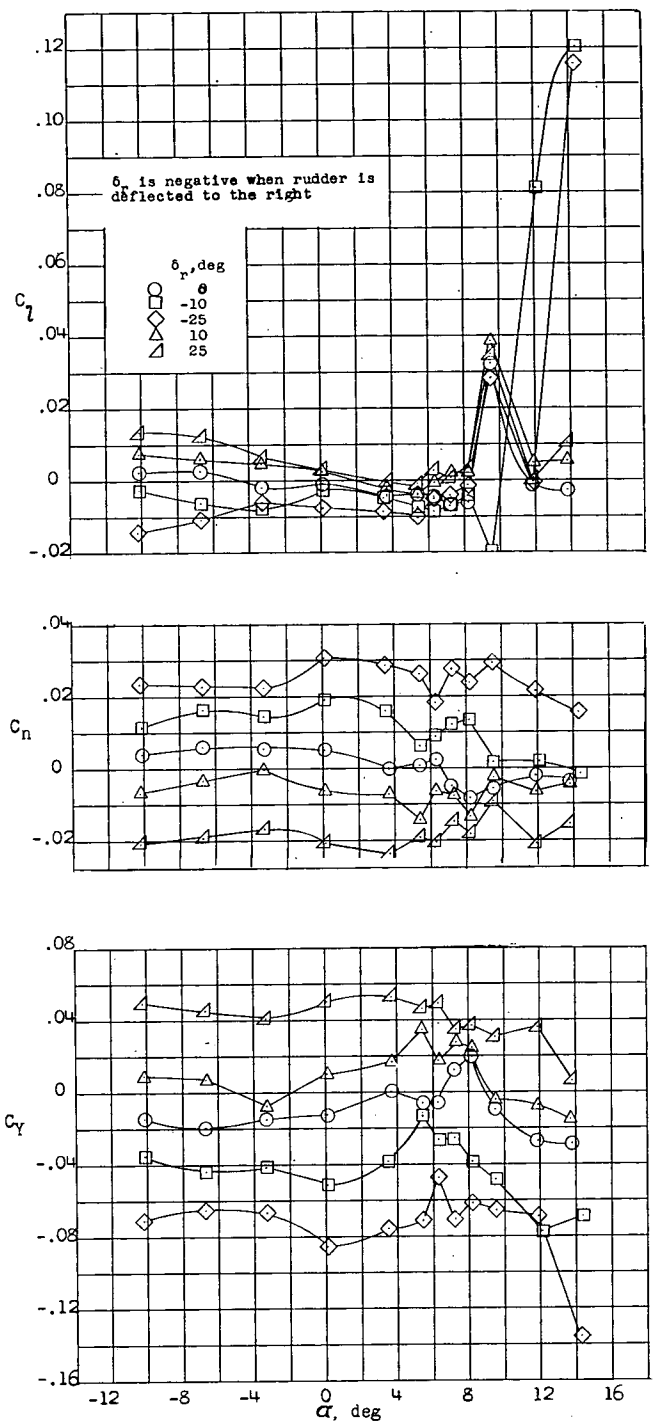


(a) Variation of $C_l$, $C_n$, and $C_Y$ with angle of attack for windmilling propeller.

Figure 19.- Effect of rudder deflection on the lateral characteristics of the model. $\psi = 0^o$.

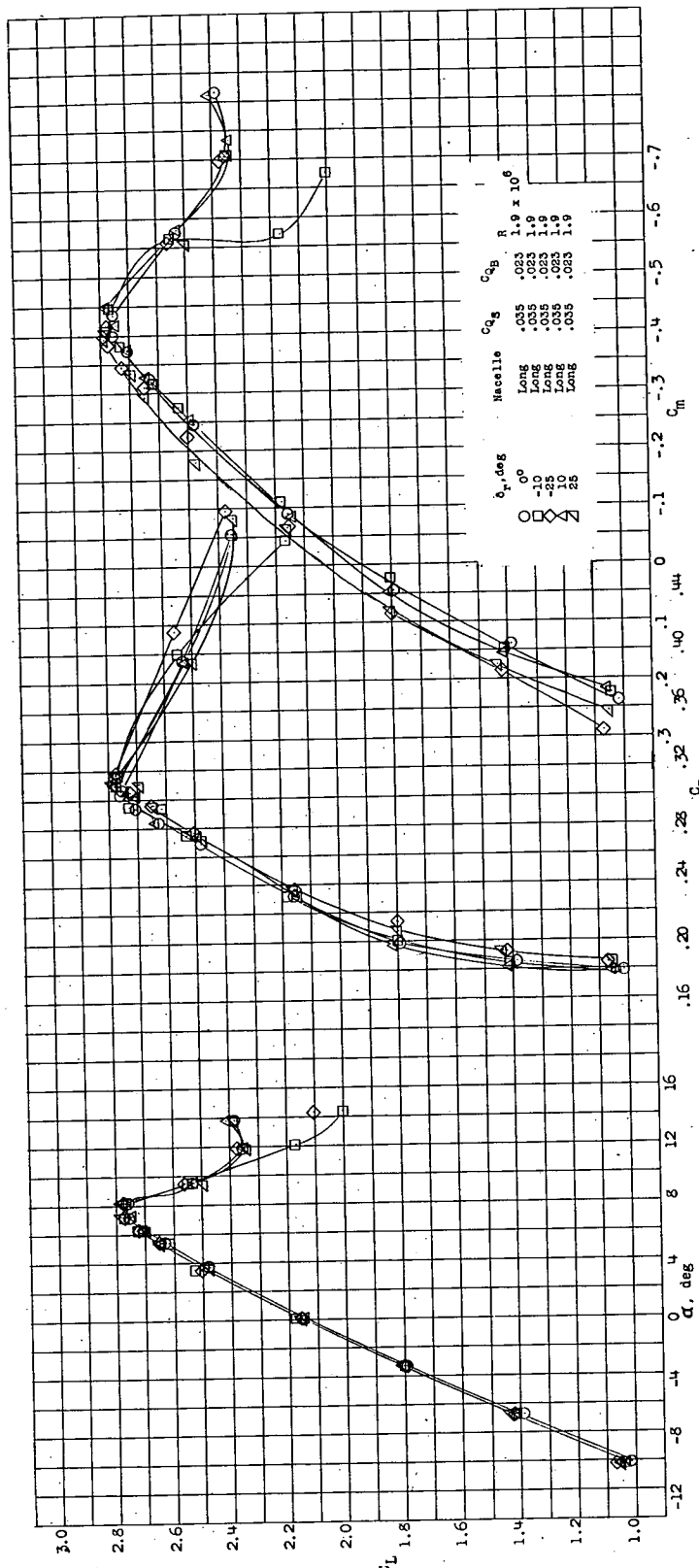


(a) Concluded. Variation of α, $C_D$, and $C_m$ with $C_L$ for windmilling propeller.

Figure 19.- Continued.

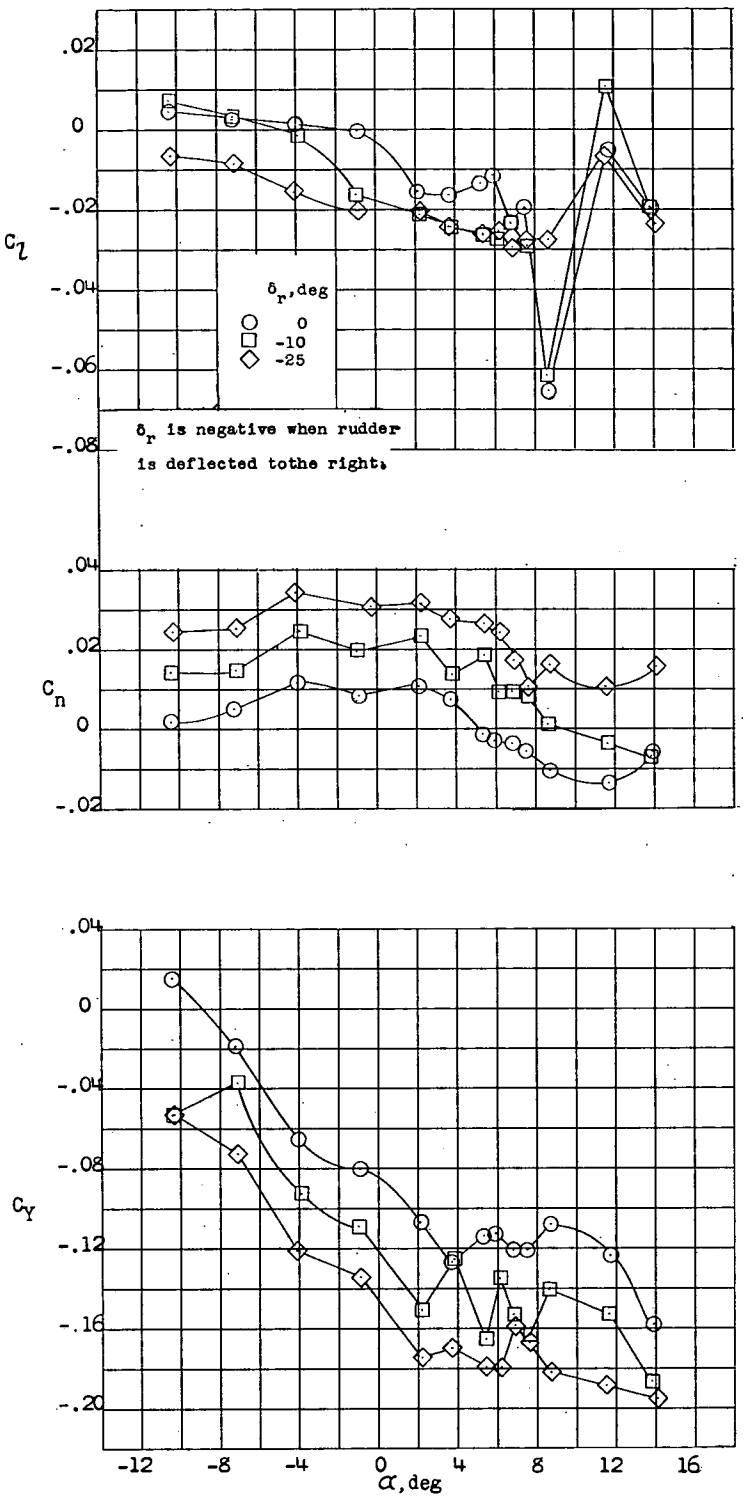


(b) Variation of $C_l$, $C_n$, and $C_Y$ with angle of attack for full power.

Figure 19.- Continued.

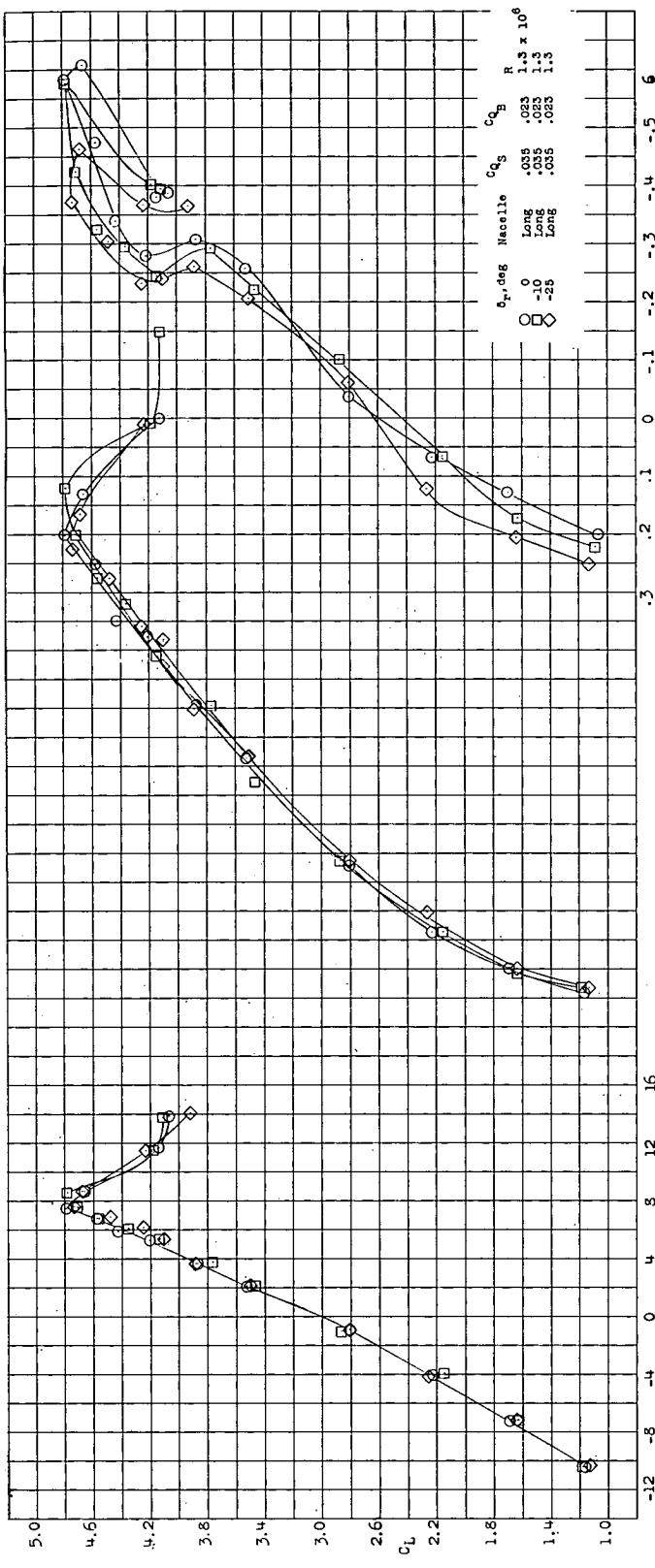


(b) Concluded. Variation of $\alpha$, $C_D$, and $C_m$ with $C_L$ for full power.

Figure 19.- Continued.

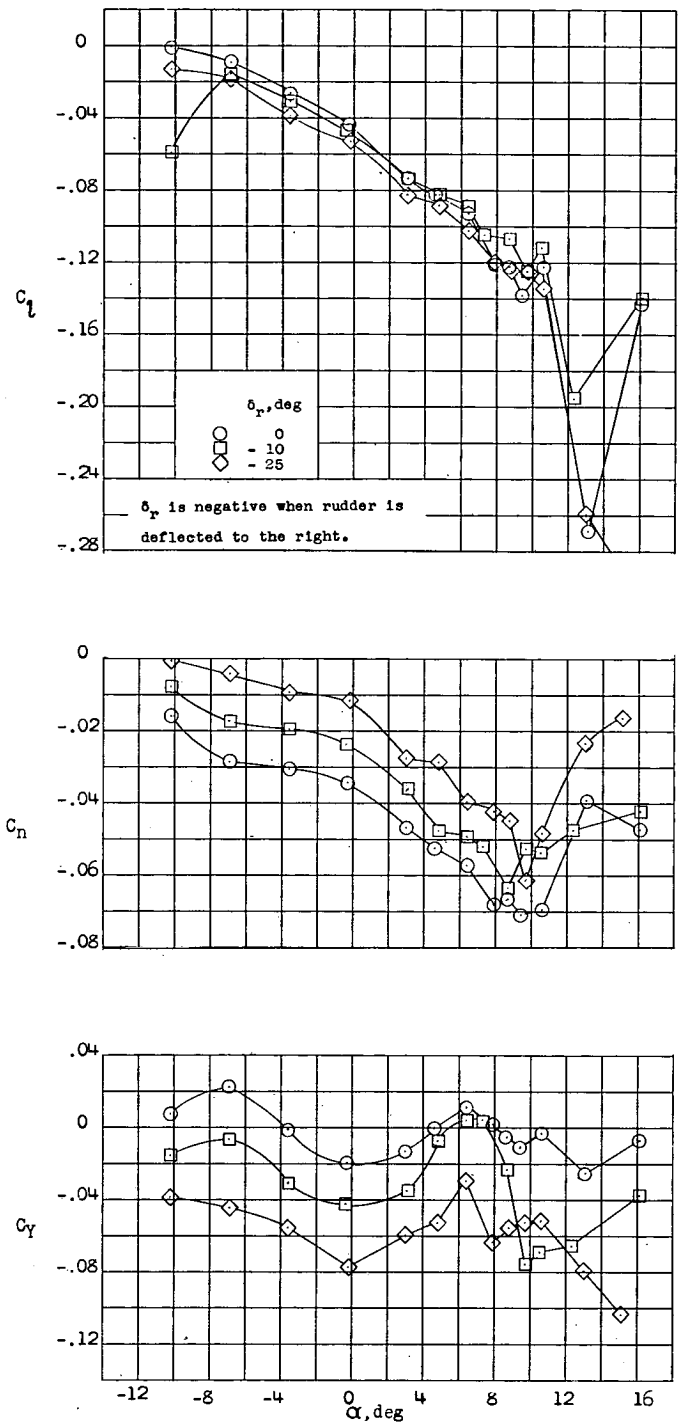


(c) Variation of $C_l$, $C_n$, and $C_Y$ with angle of attack for asymmetric power. (Full power on right side.)

Figure 19.- Continued.

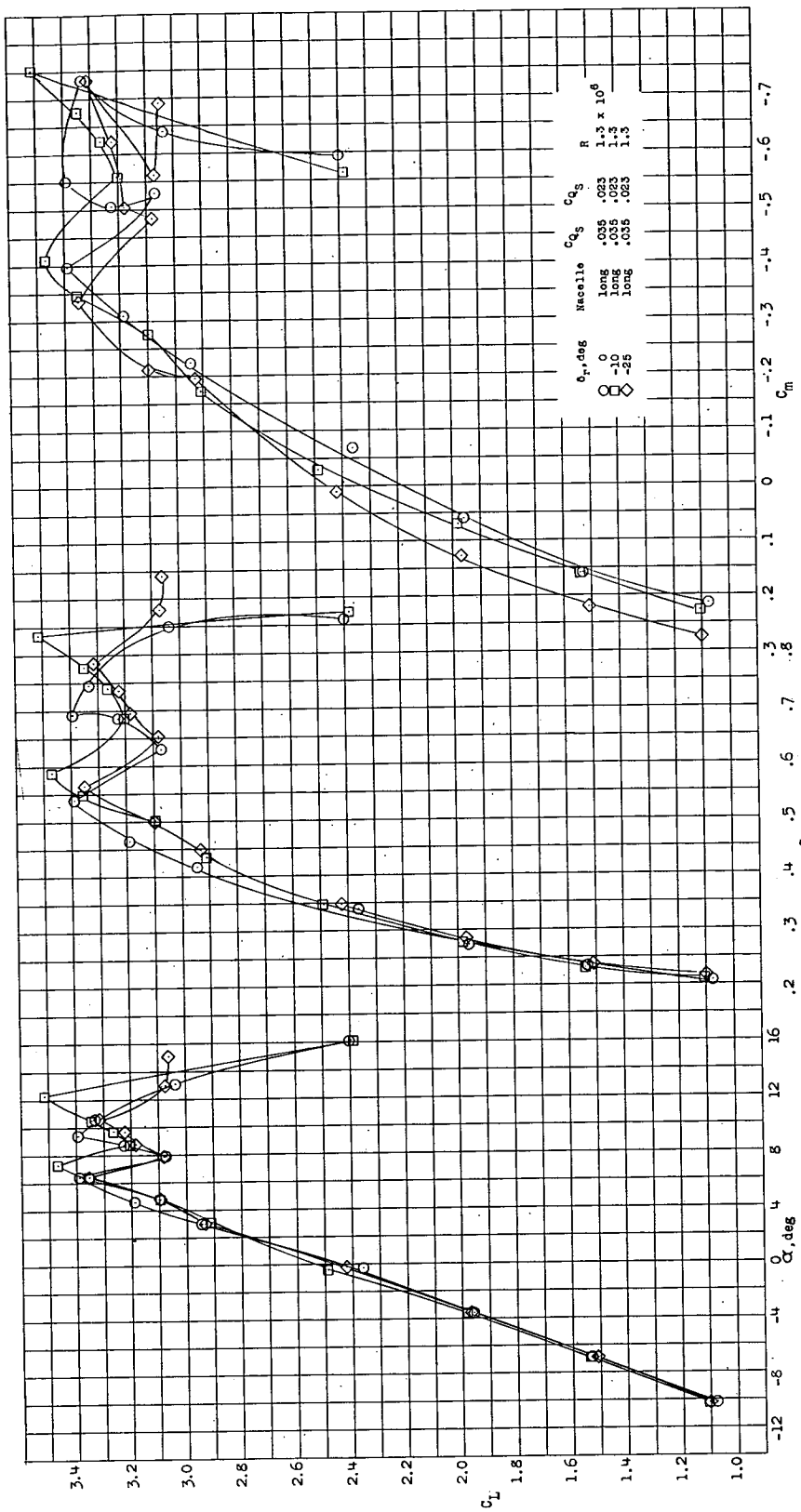


(c) Concluded. Variation of $\alpha$, $C_D$, and $C_m$ with $C_L$ for asymmetric power. (Full power on right side.)

Figure 19.- Concluded.

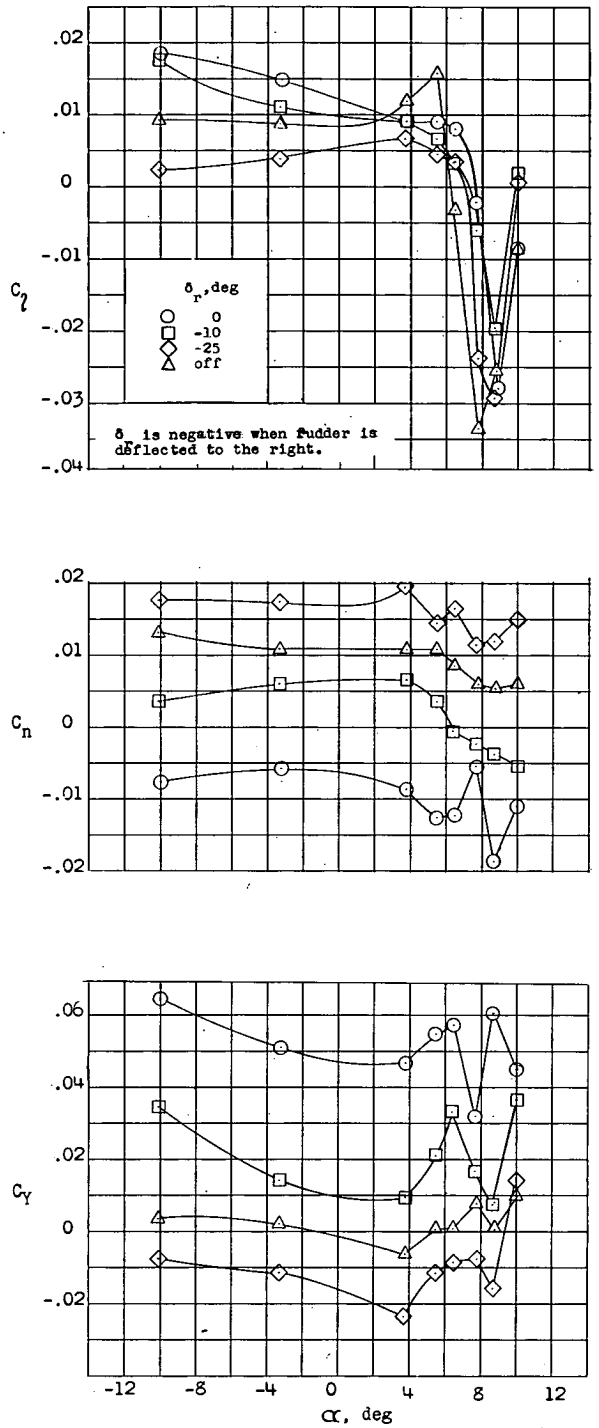


(a) Variation of $C_l$, $C_n$, and $C_Y$ with angle of attack for windmilling propeller. $\psi = 9.85^\circ$.

Figure 20.- Effect of rudder deflection on the model characteristics in yaw.

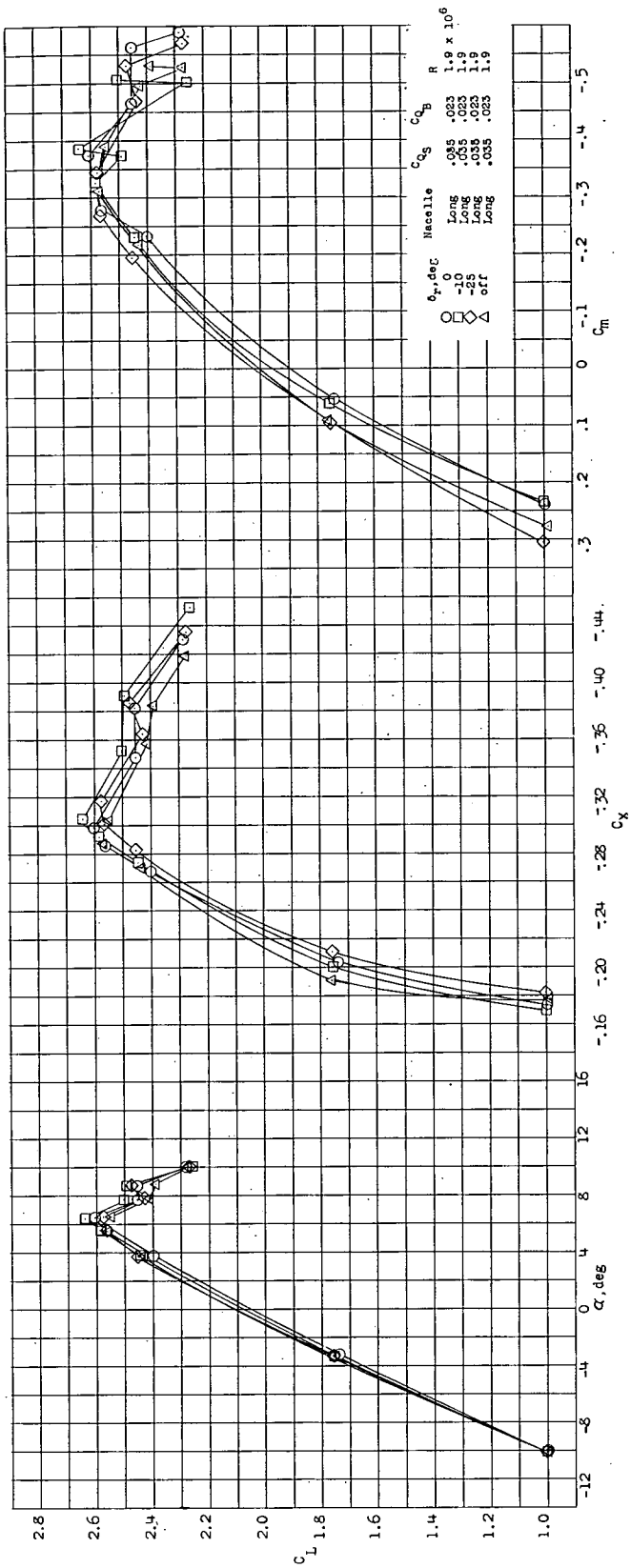


(a) Concluded. Variation of $\alpha$, $C_D$, and $C_m$ with $C_L$ for windmilling propeller. $\psi = 9.85°$.

Figure 20.- Continued.

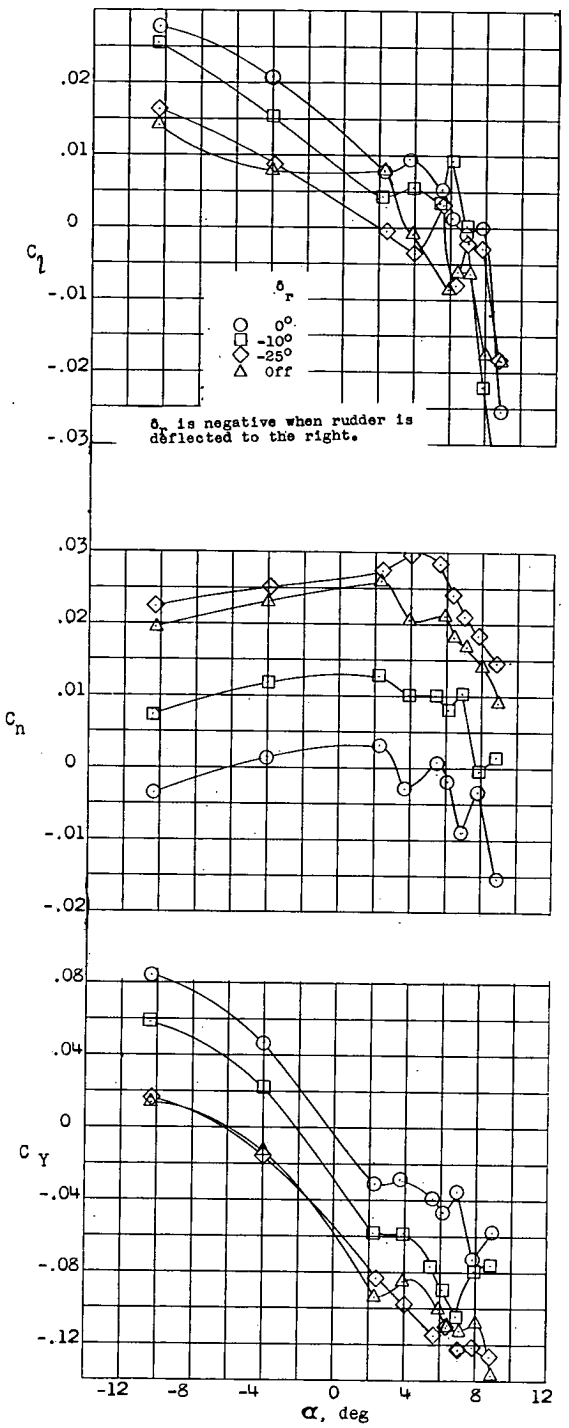


(b) Variation of $C_l$, $C_n$, and $C_Y$ with angle of attack for full power. $\psi = 9.85°$.

Figure 20.- Continued.

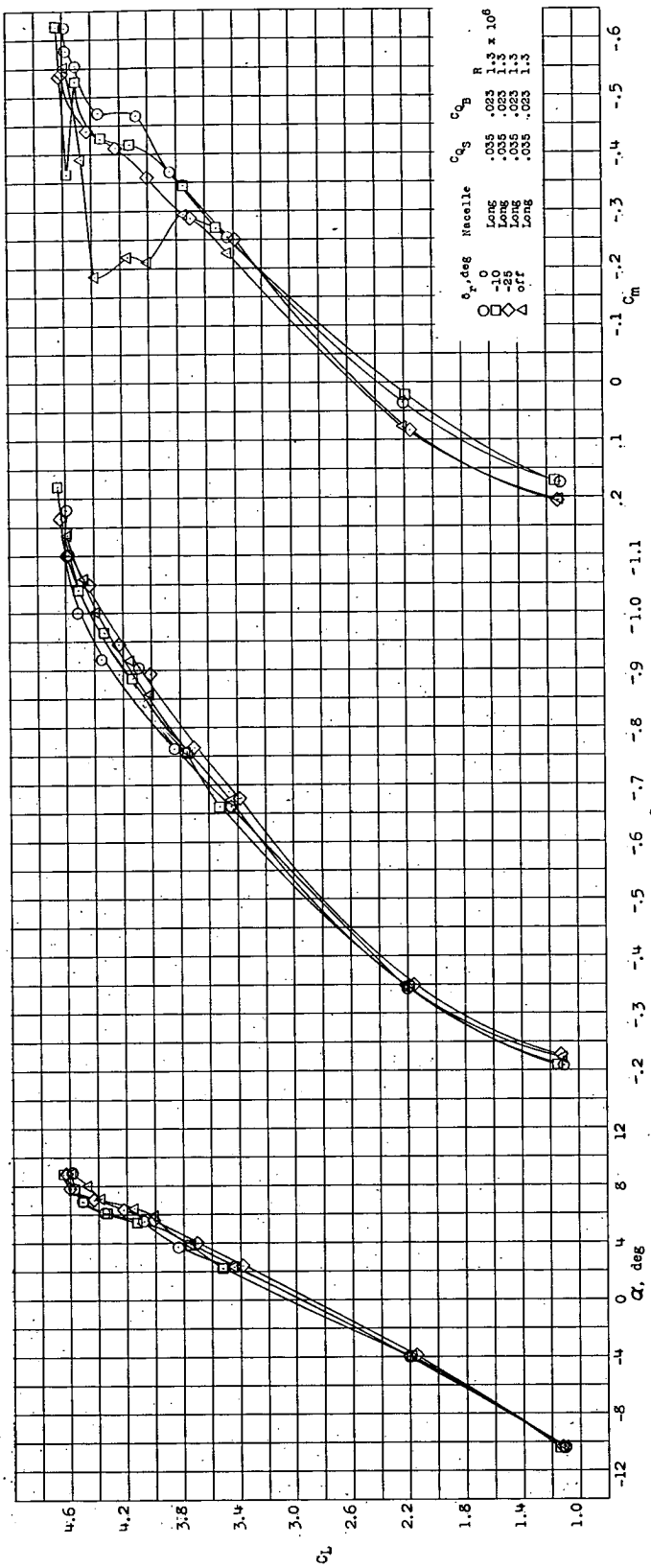


(b) Concluded. Variation of $\alpha$, $C_D$, and $C_m$ with $C_L$ for full power. $\psi = 9.85°$.

Figure 20.- Continued.

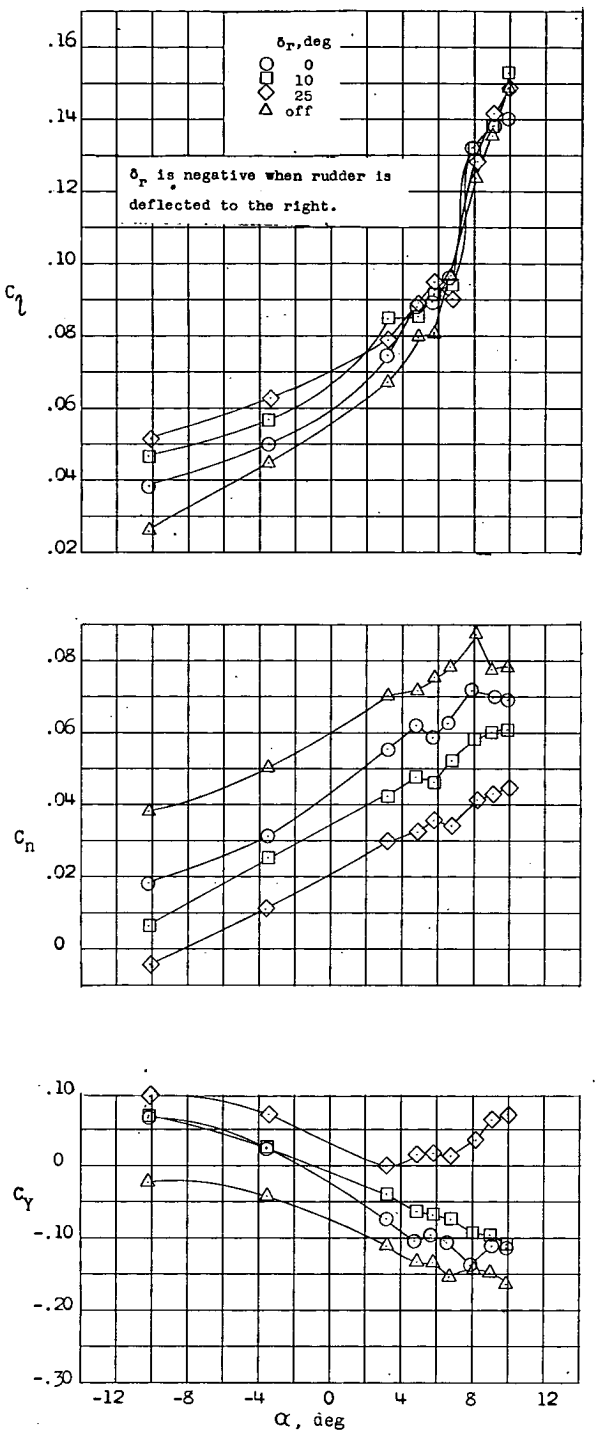


(c) Variation of $C_l$, $C_n$, and $C_Y$ with angle of attack for asymmetric power and $\psi = 9.85^\circ$. (Full power on left side.)

Figure 20.- Continued.

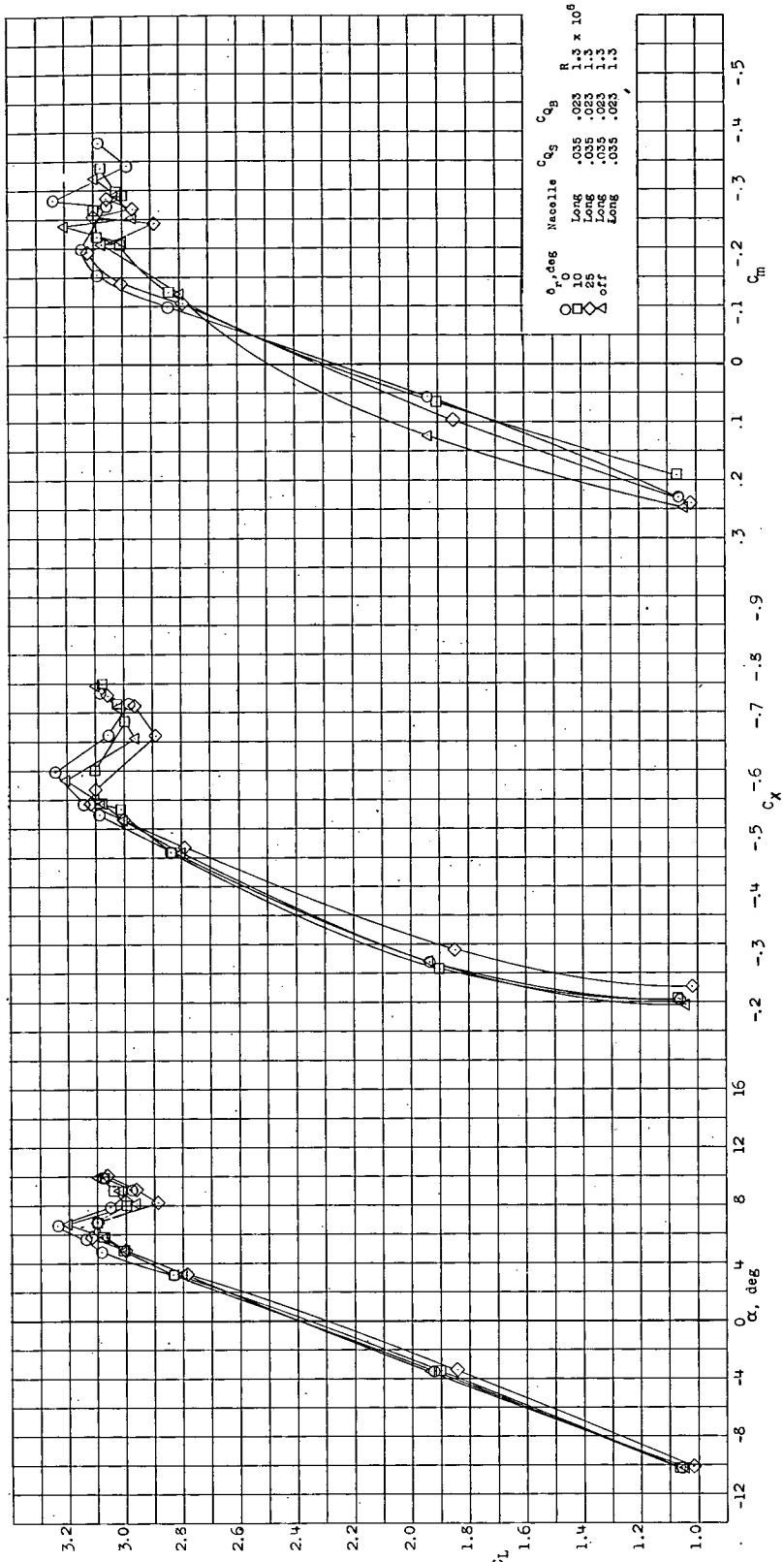


(c) Concluded. Variation of $\alpha$, $C_D$, and $C_m$ with $C_L$ for asymmetric power and $\psi = 9.85°$. (Full power on left side.)

Figure 20.- Concluded.

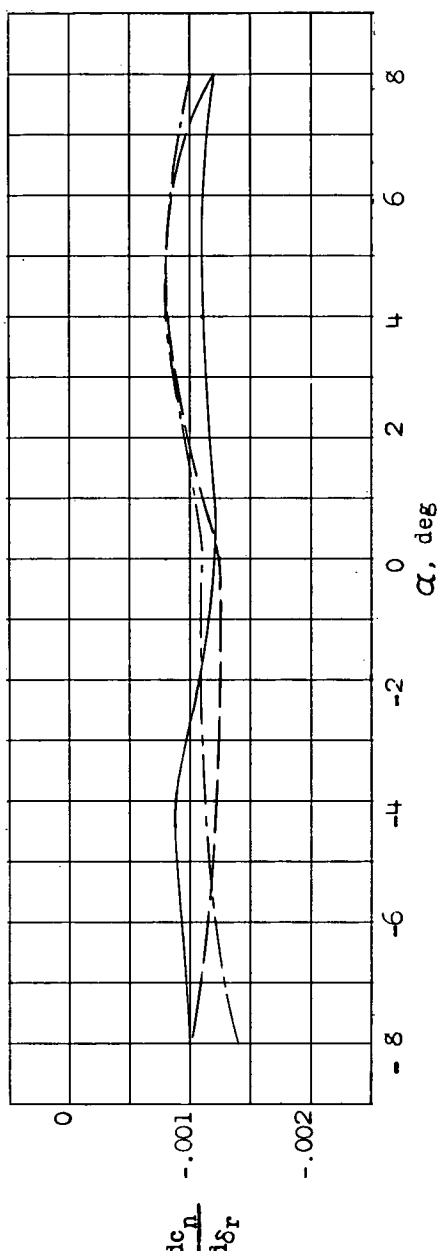


(a) Rudder effectiveness for $\psi = 0^\circ$.

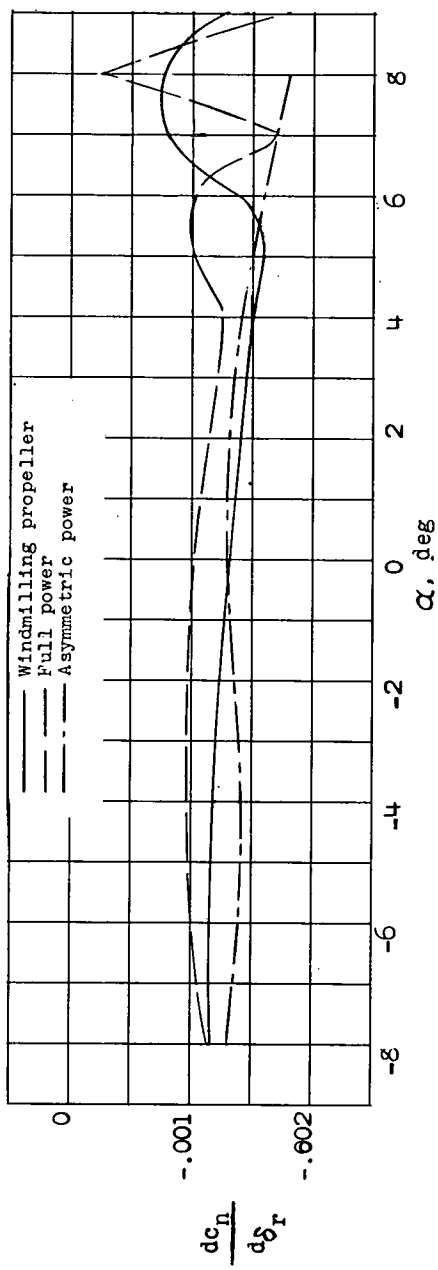


(b) Rudder effectiveness for $\psi = 9.85^\circ$.

Figure 21.- Variation of rudder effectiveness parameter with angle of attack for several power conditions and yaw angles.